

# NWP SAF

## *Satellite Application Facility for Numerical Weather Prediction*

Document NWPSAF-KN-TR-002

Version 1.2

31-08-2006

## On the quality of high resolution wind fields

*Jur Vogelzang*

***KNMI, De Bilt, The Netherlands***



<b>NWP SAF</b>	<b>On the quality of high resolution wind fields</b>	Doc ID : NWPSAF-KN-TR-002 Version : 1.2 Date : 31-08-2006
----------------	--	---

On the quality of high resolution wind fields  
Jur Vogelzang  
KNMI, De Bilt, The Netherlands

This documentation was developed within the context of the EUMETSAT Satellite Application Facility on Numerical Weather Prediction (NWP SAF), under the Cooperation Agreement dated 16 December, 2003, between EUMETSAT and the Met Office, UK, by one or more partners within the NWP SAF. The partners in the NWP SAF are the Met Office, ECMWF, KNMI and Météo France.

**Copyright 2006, EUMETSAT, All Rights Reserved.**

Change record				
Version	Date	Author	Approved	Remarks
1.0	June 2006	Jur Vogelzang	--	First draft
1.1	July 2006	Jur Vogelzang	--	Second draft, for approval
1.2	August 2006	Jur Vogelzang	Ad Stoffelen	Final version

# Contents

<b>1</b>	<b>Introduction</b> .....	<b>1</b>
<b>2</b>	<b>Statistics and spectrum</b> .....	<b>5</b>
2.1	Definitions and approach .....	5
2.2	Implementation .....	12
2.3	The effect of noise on the autocorrelation .....	14
2.4	The effect of a finite interval on the spectrum .....	16
<b>3</b>	<b>Results for the autocorrelation</b> .....	<b>21</b>
3.1	The SeaWinds dataset .....	21
3.2	Standard results .....	22
3.3	Geographical zone, WVC, and orbit .....	25
3.4	Multi Solution Scheme (MSS) .....	30
<b>4</b>	<b>Quantification of the noise level</b> .....	<b>33</b>
4.1	Estimation of the noise peak height .....	33
4.2	Standard results .....	37
4.3	Orbit and geographical zone .....	38
4.4	Minimization routine .....	38
4.5	MSS .....	39
4.6	Resolution .....	40
<b>5</b>	<b>Results for the spectrum</b> .....	<b>43</b>
5.1	Comparison of methods .....	43
5.2	Window function .....	44
<b>6</b>	<b>Comparison with DIRTH</b> .....	<b>47</b>
<b>7</b>	<b>Outlook to the Future</b> .....	<b>49</b>
<b>8</b>	<b>Conclusions</b> .....	<b>51</b>
	<b>References</b> .....	<b>53</b>

<b>NWP SAF</b>	<b>On the quality of high resolution wind fields</b>	Doc ID : NWPSAF-KN-TR-002 Version : 1.2 Date : 31-08-2006
----------------	--	---

NWP SAF	<b>On the quality of high resolution wind fields</b>	Doc ID : NWPSAF-KN-TR-002 Version : 1.2 Date : 31-08-2006
---------	--	---

# 1 Introduction

The Seawinds Data Processor (SDP) is a software package that processes data from the SeaWinds scatterometer instrument on board the QuikSCAT satellite to wind vectors on a regular grid [SCAT group, 2006a]. SDP is a deliverable within the Initial Operations Phase (IOP) of the Eumetsat project NWP SAF. SDP features new and improved techniques, in particular:

- Multi Solution Scheme (MSS);
- 2D Variational Ambiguity Removal (2DVAR);
- selectable size for the wind vector cells (100 km, 50 km, or 25 km).

In the MSS up to 144 solutions and their relative probability are retained rather than the usual choice of 4 solutions at most represented by minima in the distance to the Geophysical Model Function (GMF). This enables the Ambiguity Removal to select a solution that, though not exactly a minimum in the distance to the GMF, has relatively high probability and fits well with other information. In 2DVAR the most probable solution is selected by minimizing a cost function that takes physical constraints (meteorological balance) into account, resulting in a consistent solution.

The quality of the SDP output has been checked against that of its predecessor, QDP, at a resolution of 100 km, and was found to be in order. The quality at 50 km and 25 km resolution, however, has not yet been established. Such a study is part of the NWP SAF project (work package 416000). The results are reported in this document.

There are in principle two ways of determining the quality of the high resolution SDP wind data: comparison with other wind data (like the triple collocation method) or investigation of the statistical properties of the SDP wind field. The latter approach has been adopted here by investigating the autocorrelation and the spectrum of the wind field.

Chapter 2 contains the basic definitions and formulas for the autocorrelation and the spectrum. The autocorrelation can be defined as a function of relative position (which can be negative) or as a function of distance. It is shown that these two approaches are identical for large data sets. It is also shown that the autocorrelation function has a discontinuity at zero distance (the so-called noise peak) if the signal contains white noise, and that the size of the discontinuity is proportional to the noise level. A noise component will flatten the spectrum at high spatial frequencies, but it is shown from an analytical example that aliasing may cause a similar effect. If the

<b>NWP SAF</b>	<b>On the quality of high resolution wind fields</b>	Doc ID : NWPSAF-KN-TR-002 Version : 1.2 Date : 31-08-2006
----------------	--	---

autocorrelation does not approach zero fast enough on its definition interval, the spectrum may contain oscillations which can be mitigated by using a Hanning filter.

Chapter 3 contains the results for the autocorrelation. The autocorrelations of the NCEP model winds, used to initialise the 2DVAR, appear continuous. The autocorrelations of the SDP wind field show a noise peak at zero distance. The effect of orbit selection, geographical zone, and wind vector cell is investigated. As can be expected, the noise peak is highest for the nadir part of the swath, where the observation geometry is less favourable. The noise peak disappears when using MSS.

In chapter 4 the standard deviation of the noise is estimated from the noise peak height. As expected, the noise level is highest in the nadir part of the swath. At 25 km resolution the standard deviation of the noise may be up to 1.4 m/s in each of the wind components  $u$  and  $v$ . The noise level varies very little with the orbit selection (ascending or descending), the geographical zone, and the choice of minimisation routine in 2DVAR. The noise level decreases with increasing wind vector cell size and becomes negligible at 100 km resolution – the resolution with which the comparison with QDP was made. The noise becomes insignificant at all resolutions if the MSS is used.

Chapter 5 contains the results for the spectra. The spectra may become rather noisy, especially for the NCEP model winds, probably due to the use of a finite interval. Application of a Hanning window smoothens the spectra, and seems to be the best choice. However, all spectra flatten at high spatial frequencies, most probably due to aliasing.

In chapter 6 the method of estimating the noise level from the autocorrelation is applied to compare KNMI's 2DVAR ambiguity removal method (with or without MSS) to the DIRTH ambiguity removal method used by NOAA. It is shown that the scatterometer winds retrieved with DIRTH contain more noise than 2DVAR with MSS, but less than 2DVAR without MSS.

Chapter 7 contains a short discussion on how to apply the results in this study in future investigations within the NWP SAF project aiming at further improvement of scatterometer wind processors. Especially study of the along track and across track wind components may be useful for more precise determination of the error covariance functions in 2DVAR.

The conclusions are listed in chapter 8. All relevant information on the quality of the wind field can be obtained from the behaviour of the autocorrelation function at short distances. The spectrum is more difficult to interpret. When calculating high resolution scatterometer wind fields one should use the MSS to avoid significant noise contributions.

NWP SAF	<b>On the quality of high resolution wind fields</b>	Doc ID : NWPSAF-KN-TR-002 Version : 1.2 Date : 31-08-2006
---------	--	---

## 2 Statistics and spectrum

This chapter contains the theoretical background needed in the rest of this report. It starts with the definition of the autocorrelation. It may be defined in two ways, as a function of position difference or as a function of distance, but it is shown that these are equivalent for large datasets. In this study the autocorrelation employed will be a function of distance.

The spectrum is defined, and its numerical implementation is discussed. A simple example shows that a Gaussian transforms into a Gaussian and a delta function into a constant. Note that white noise also has a constant spectrum, so a white noise component should show up as a delta function in the autocorrelation.

It is shown that indeed a white noise component causes a discontinuity in the autocorrelation at zero distance. The height of this discontinuity is proportional to the noise variance, with the total variance as constant of proportionality. An estimation of the size of the discontinuity thus allows calculation of the noise level, as will be done in chapter 4.

In chapter 3 it will be shown that the autocorrelation for scatterometer wind fields approaches zero very slowly. Therefore the spectrum may be affected by numerical effects. Using an analytical example, these effects are studied in section 2.4. It is shown that poor cutoff due to the definition of the autocorrelation on a finite interval causes an oscillation in the spectrum. The numerical (FFT) method also suffers from aliasing in the high frequency part, causing the spectrum to flatten in a way indiscernible from a white noise contribution. Application of a Hanning window removes the oscillations, but not the aliasing.

### 2.1 Definitions and approach

Suppose we have a finite set of spatial varying data  $\{v_i\} = \{v(x_i)\}$ . There are many statistical quantities to characterize such a dataset. The most common are the mean, or first moment, and the second moment,  $M_X$  and  $M_{XX}$  respectively, defined as

$$M_X = \frac{1}{N} \sum_{i=1}^N v_i \quad , \quad (2.1)$$

$$M_{XX} = \frac{1}{N} \sum_{i=1}^N v_i^2 \quad . \quad (2.2)$$

The variance  $\sigma^2$  of the set equals

<b>NWP SAF</b>	<b>On the quality of high resolution wind fields</b>	Doc ID : NWPSAF-KN-TR-002 Version : 1.2 Date : 31-08-2006
----------------	--	---

$$\sigma^2 = \frac{1}{N} \sum_{i=1}^N [v_i^2 - M_X^2] = M_{XX} - M_X^2 \quad (2.3)$$

For the autocorrelation one must consider pairs of data and construct statistics over the pairs as a function of the distance between the members of the pair. There are two ways to define the pairs: the directional approach and the distance approach.

In the directional approach the set of pairs  $P(s)$  is defined as

$$P(s) = \{(v_i, v_j) \mid x_i - x_j = s\} \quad (2.4)$$

where  $s$  may be positive (for  $x_i > x_j$ ) or negative (for  $x_i < x_j$ ). It is also possible to define the autocorrelation as a function of the distance between the members of the pair,

$$\bar{P}(r) = \{(v_i, v_j) \mid \|x_i - x_j\| = r\} \quad (2.5)$$

A pair  $(v_i, v_j)$  contributes once to  $P(s)$ , because the pair  $(v_j, v_i)$  contributes to  $P(-s)$ , while it contributes twice to  $\bar{P}(\|s\|) = \bar{P}(r)$ : once as  $(v_i, v_j)$  and once as  $(v_j, v_i)$ . The number of pairs in  $\bar{P}(r)$  is therefore twice the number of pairs in  $P(s)$  for  $s = r$ .

### Directional approach

In the directional approach there is a distinction between the first and second point of a pair. To take this distinction into account, the subscript  $X$  is used to denote the first member of the pair, while the subscript  $Y$  denotes the second member. The first moments with respect to the first and second members of each pair are

$$M_X(s) = \frac{1}{N(s)} \sum_{P(s)} v_i \quad (2.6a)$$

$$M_Y(s) = \frac{1}{N(s)} \sum_{P(s)} v_j \quad (2.6b)$$

respectively, with  $v_i$  the first point of a contributing pair,  $v_j$  the second point, and  $N(s)$  the number of pairs in  $P(s)$ . The set  $P(s)$  consists of all pairs  $(x_i, x_j)$  with  $x_i - x_j = s$  as defined in (2.4).

The second moments are defined in a similar way:

$$M_{XX}(s) = \frac{1}{N(s)} \sum_{P(s)} v_i^2 \quad (2.7a)$$

$$M_{YY}(s) = \frac{1}{N(s)} \sum_{P(s)} v_j^2 \quad (2.7b)$$

<b>NWP SAF</b>	<b>On the quality of high resolution wind fields</b>	Doc ID : NWPSAF-KN-TR-002 Version : 1.2 Date : 31-08-2006
----------------	--	---

One can also define a mixed second moment  $M_{XY}(s)$  according to

$$M_{XY}(s) = \frac{1}{N(s)} \sum_{P(s)} v_i v_j \quad , \quad (2.8)$$

The variances are defined as

$$\sigma_X^2(s) = \frac{1}{N(s)} \sum_{P(s)} [v_i^2 - M_X^2(s)] = M_{XX}(s) - M_X^2(s) \quad , \quad (2.9a)$$

$$\sigma_Y^2(s) = \frac{1}{N(s)} \sum_{P(s)} [v_i^2 - M_Y^2(s)] = M_{YY}(s) - M_Y^2(s) \quad , \quad (2.9b)$$

and the covariance  $C(s)$  is

$$C(s) = \frac{1}{N(s)} \sum_{P(s)} [v_i v_j - M_X(s)M_Y(s)] = M_{XY}(s) - M_X(s)M_Y(s) \quad . \quad (2.10)$$

The autocorrelation  $\rho(s)$  reads

$$\rho(s) = \frac{C(s)}{\sigma_X(s)\sigma_Y(s)} \quad . \quad (2.11)$$

Note that the autocorrelation is an even function,  $\rho(-s) = \rho(s)$ , and that  $\rho(0) = 1$  by definition.

The first moments  $M_X(s)$  and  $M_Y(s)$  in (2.6a) and (2.6b) differ from each other because they are obtained from a different set of points. They also differ from the first moment of the complete dataset defined in (2.1) because the set  $P(s)$  is generally a subset of the complete dataset. For  $s=0$  the set  $P(0)$  equals the whole dataset and  $N(0) = N$ . In that case  $M_X = M_Y$ ,  $M_{XX} = M_{XY} = M_{YY}$ , and the covariance (2.10) equals the variances (2.9a) and (2.9b).

## Distance approach

In the distance approach the moments and the autocorrelation are functions of the distance  $r = \|s\|$ . They are defined in a similar manner as in the directional approach, see equations (2.6) – (2.11), but now the summations are over the set  $\bar{P}(r)$  defined in (2.5). The first moments satisfy, the bar denoting the distance approach

$$\overline{M_X}(r) = \frac{1}{\overline{N}(r)} \sum_{\bar{P}(r)} v_i \quad , \quad (2.12a)$$

$$\overline{M_Y}(r) = \frac{1}{\overline{N}(r)} \sum_{\bar{P}(r)} v_j \quad . \quad (2.12b)$$

Since each pair  $(v_i, v_j)$  also contributes as  $(v_j, v_i)$ , the first moments  $\overline{M_X}$  and  $\overline{M_Y}$  are identical. This can be seen readily for a small dataset. The same holds for the second moments:

<b>NWP SAF</b>	<b>On the quality of high resolution wind fields</b>	Doc ID : NWPSAF-KN-TR-002 Version : 1.2 Date : 31-08-2006
----------------	--	---

$\overline{M_{XX}} = \overline{M_{YY}}$ . Therefore the definition of the autocorrelation (2.11) simplifies in the distance approach to

$$\overline{\rho}(r) = \frac{\overline{C}(r)}{\overline{\sigma}^2(r)} \quad . \quad (2.13)$$

with

$$\overline{\sigma}^2(r) = \overline{M_{XX}}(r) - \overline{M_X}^2(r) \quad , \quad (2.14)$$

$$\overline{C}(r) = \overline{M_{XY}}(r) - \overline{M_X}^2(r) \quad , \quad (2.15)$$

and

$$\overline{M_X}(r) = \frac{1}{N(r) P(r)} \sum v_i \quad , \quad (2.16)$$

$$\overline{M_{XX}}(r) = \frac{1}{N(r) P(r)} \sum v_i^2 \quad , \quad (2.17)$$

$$\overline{M_{XY}}(r) = \frac{1}{N(r) P(r)} \sum v_i v_j \quad , \quad (2.18)$$

with  $\overline{P}(r)$  defined according to (2.5) as the set of pairs  $(v_i, v_j)$  for which  $\|x_i - x_j\| = r$ . As in the directional approach,  $\overline{\rho}(0) = 1$  by definition.

## Equivalence of the two approaches

Consider for a moment only positive values for  $s$  and suppose we have a set of equally spaced data  $\{v_i\} = \{v(x_i)\}$  with  $x_i = i\Delta$ ,  $i = 1, 2, \dots, N$ . Consider now the statistics for distance  $\Delta$ , so the pairs are formed by adjacent points.

In the directional approach, the pairs for  $s = \Delta$  are

$$P(\Delta) = \{(v_2, v_1), (v_3, v_2), \dots, (v_{N-1}, v_{N-2}), (v_N, v_{N-1})\} \quad . \quad (2.19)$$

There are  $N(\Delta) = N - 1$  pairs and the first moments in the directional approach can be written as

$$M_X(\Delta) = \frac{1}{N-1} \sum_{i=2}^N v_i = A + \frac{v_N}{N-1} \quad , \quad (2.20)$$

$$M_Y(\Delta) = \frac{1}{N-1} \sum_{i=1}^{N-1} v_i = A + \frac{v_1}{N-1} \quad , \quad (2.21)$$

where

<b>NWP SAF</b>	<b>On the quality of high resolution wind fields</b>	Doc ID : NWPSAF-KN-TR-002 Version : 1.2 Date : 31-08-2006
----------------	--	---

$$A = \frac{1}{N-1} \sum_{i=2}^{N-1} v_i \quad , \quad (2.22)$$

is the overlap between (2.20) and (2.21). See also figure 2.1 for a graphical illustration. For a sufficient large dataset,  $N \rightarrow \infty$ , the contribution of the non-overlapping terms vanishes and the moments become equal. The same holds for other values of the argument and for the second order moments.

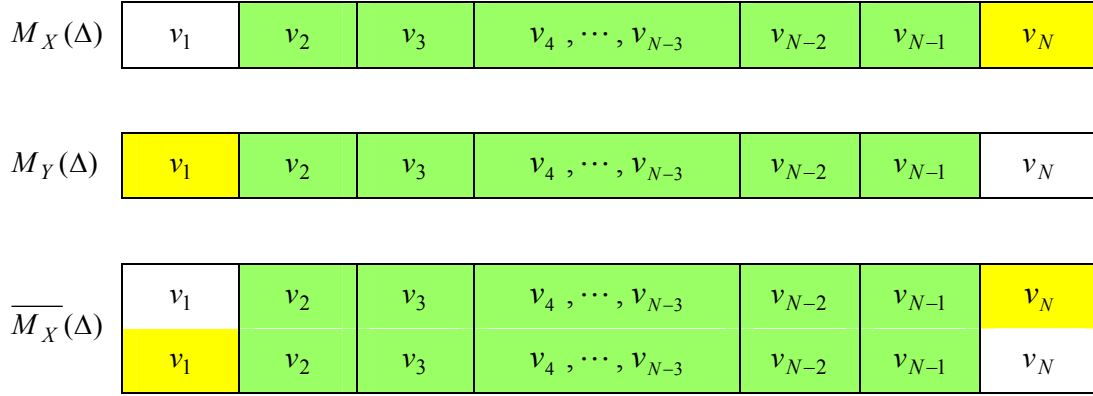


**Figure 2.1** Terms contributing to the first order moments in the directional approach (upper and middle) and the distance approach (lower). The overlapping contributing terms are marked in green, the non-overlapping ones in yellow.

For  $s = -\Delta$  the members of each pair change order, and the pairs are

$$P(-\Delta) = \{(v_1, v_2), (v_2, v_3), \dots, (v_{N-2}, v_{N-1}), (v_{N-1}, v_N)\} \quad . \quad (2.23)$$

The first moments read

$$M_X(-\Delta) = \frac{1}{N-1} \sum_{i=1}^{N-1} v_i = M_Y(\Delta) \quad , \quad (2.24)$$

$$M_Y(-\Delta) = \frac{1}{N-1} \sum_{i=2}^N v_i = M_X(\Delta) \quad . \quad (2.25)$$

This also holds for other values of the arguments and for higher order moments.

In the distance approach, the pairs are

$$\bar{P}(\Delta) = \{(v_2, v_1), (v_1, v_2), (v_3, v_2), (v_2, v_3), \dots, (v_N, v_{N-1}), (v_{N-1}, v_N)\} \quad . \quad (2.26)$$

The are  $\bar{N}(\Delta) = 2(N-1)$  pairs, and the first moment in the distance approach reads

$$\bar{M}_X(\Delta) = \frac{1}{2(N-1)} \sum_{i=2}^N (v_i + v_{i-1}) = \frac{1}{2(N-1)} \left[ \sum_{i=2}^N v_i + \sum_{i=1}^{N-1} v_i \right] \quad . \quad (2.27)$$

<b>NWP SAF</b>	<b>On the quality of high resolution wind fields</b>	Doc ID : NWPSAF-KN-TR-002 Version : 1.2 Date : 31-08-2006
----------------	--	---

Using (2.20), (2.21) and (2.24) this can be rewritten as

$$\overline{M_X}(\Delta) = \frac{1}{2} [M_X(\Delta) + M_Y(\Delta)] = \frac{1}{2} [M_X(\Delta) + M_X(-\Delta)] \quad . \quad (2.28)$$

The first order moment in the distance approach is the average of the two first order moments in the directional approach, or, equivalently, the average of the first moment in the distance approach at positive and negative values of the argument. For large data sets the difference between the three first order moments vanishes. The same holds for other values of the argument and for the second order moments. Therefore the two approaches are equivalent.

## Spectrum

The one-sided power spectral density  $\Psi(k)$  is defined as the absolute value squared of the Fourier transform of the autocorrelation function according to

$$\Psi(k) = \left| \int_{-\infty}^{\infty} dr \rho(r) e^{2\pi i k r} \right|^2 \quad . \quad (2.29)$$

with the spatial frequency  $k = x^{-1}$ . Note that  $k$  is a scaled spatial wave number because the factor  $2\pi$  has been incorporated in the exponential of (2.29).

## 2.2 Implementation

In this study the data will be on a regular grid with grid size  $\Delta$ , so

$$r = x_i - x_j = (i - j)\Delta = k\Delta \quad , \quad (x_i, x_j) \in P(r) \quad . \quad (2.30)$$

Therefore the distance between the members of data pairs, and thus all statistics derived from them, are characterized by a single integer  $l$ . We will follow the distance approach, so only positive values of  $k$ , because it requires less storage and is computationally more efficient than the directional approach. Apparently, the distance approach gives better statistics because the number of pairs  $\overline{P}(r)$  is twice the number of pairs in the directional approach  $P(r)$ . However, as shown in section 2.2 this is just a matter of definition: the pairs may be counted twice but no extra independent information is added.

The autocorrelations were calculated using the routines and data structures in the AutoCorrelationMod module of KNMI's genscat library. This module requires that the data are

<b>NWP SAF</b>	<b>On the quality of high resolution wind fields</b>	Doc ID : NWPSAF-KN-TR-002 Version : 1.2 Date : 31-08-2006
----------------	--	---

fed to the software one after another in the right spatial or temporal order. The moments  $S_n(l)$  obtained for  $n$  data pairs with distance  $l\Delta$  are updated according to the formula

$$S_{n+2}(l) = \frac{1}{n+2} \sum_{m=1}^{n+2} [f(v_i, v_j) + f(v_j, v_i)] = S_n(l) + \frac{f(v_i, v_j) + f(v_j, v_i) - 2S_n(l)}{n+2}, \quad (2.31)$$

where  $(v_i, v_j)$  and  $(v_j, v_i)$  are the two data pairs formed from the point  $v_i$  that is just read in and the earlier point  $v_j$  that is stored in the data structures of the module. Further,  $i - j = l$ , or, equivalently,  $j = i - l$ . The function  $f$  is defined for the first and second moments as follows

$$M_X : f(v_i, v_j) = v_i, \quad (2.32)$$

$$M_{XX} : f(v_i, v_j) = v_i^2, \quad M_{XY} : f(v_i, v_j) = v_i v_j.$$

The autocorrelation is calculated according to (2.13). The routines in the AutoCorrelationMod module can handle gaps in the data by adding a suitable number of no-data points to the bookkeeping without affecting the statistics calculated so far. The number of distances taken into account,  $N$ , is a power of 2 ( $N = 128$  at 25 km resolution), though any value for  $N$  may be adopted. The maximum distance is  $R_{\max} = N\Delta x$ .

Note that the moments are updated rather than their underlying sums. This is done because updating the moments is numerically more stable for very large data sets than updating the sums, though the latter approach is simpler and computationally more efficient.

The spectrum is calculated from the autocorrelation using the FFT routines from KNMI's genscat library. The size of the FFT grid is  $N_F = 2N$ . It is filled using the scheme of table 2.1.

FFT grid point	Value
1	$\rho(K)$
2	$\rho(K-1)$
...	...
$K$	$\rho(1)$
$K+1$	$\rho(0)=1$
$K+2$	$\rho(1)$
...	...
$2K$	$\rho(K-1)$

**Table 2.1** Scheme for filling the FFT grid with autocorrelation values.

<b>NWP SAF</b>	<b>On the quality of high resolution wind fields</b>	Doc ID : NWPSAF-KN-TR-002 Version : 1.2 Date : 31-08-2006
----------------	--	---

When using this scheme, the autocorrelation is made periodical using its symmetry properties.

The spatial frequency  $k$  satisfies

$$k_j = j\Delta k \quad , \quad j = 0, \dots, N \quad , \quad (2.33)$$

with

$$\Delta k = \frac{1}{N_F \Delta x} = \frac{1}{2N\Delta x} = \frac{1}{2R_{\max}} \quad . \quad (2.34)$$

Note that  $\Delta k$  equals the inverse of the total range in position, and that  $\Delta x \Delta k = N_F^{-1}$ .

If desired, the autocorrelation values in the FFT grid may be multiplied with a window function, like the Hanning window, the Parzen Window, or the Welch window. See *Press et al.* [1988] for the definition of these window functions.

The FFT routine has been tested on functions with a Fourier transform that can be calculated analytically: the Gaussian and the Dirac delta function. Indeed a Gaussian that was not too wide or too narrow transforms into a Gaussian, and the Dirac delta function transforms into a constant, all within the expected numerical precision.

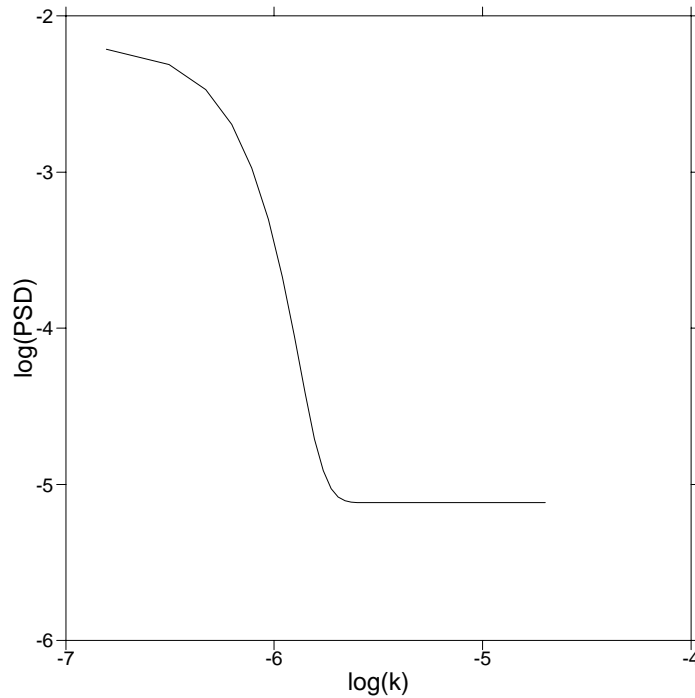


**Figure 2.2** Numerical spectrum for a combination of a Gaussian and a delta function.

<b>NWP SAF</b>	<b>On the quality of high resolution wind fields</b>	Doc ID : NWPSAF-KN-TR-002 Version : 1.2 Date : 31-08-2006
----------------	--	---

Figure 2.2 shows the spectrum of the function

$$f(x) = \begin{cases} 1 & x = 0 \\ \frac{1}{2}e^{-ax^2} & x \neq 0 \end{cases}, \quad (2.35)$$

a combination of a Gaussian and a delta function. The curve shown in figure 2.2 is the numerical result. Its relative precision compared to the analytical result is better than  $10^{-6}$ , so the analytical curve would coincide with the numerical result in figure 2.2.

The fact that a delta function transforms into a constant function is important, because the spectrum may be used to get information about the noise in the scatterometer winds. One expects a decaying spectrum (roughly proportional to  $k^{-2}$ ) that flattens and becomes constant at the noise level [Milliff, 2004; Chelton *et al.*, 2006]. However, such a feature should be visible as a delta function in the autocorrelation - a discontinuity at zero distance. This idea will be developed further in the next section.

### 2.3 The effect of noise on the autocorrelation

Suppose we have a signal  $s(r)$  that is built up from a coherent signal  $c(r)$  and a noise contribution  $n(r)$ ,  $s(r) = c(r) + n(r)$ . We assume that the noise has zero average and is completely uncorrelated. The mixed second order moment reads (omitting the bars for a moment)

$$M_{XY}[s(r)] = \frac{1}{N(r)} \sum_{P(r)} s_i s_j = \frac{1}{N(r)} \sum_{P(r)} (c_i + n_i)(c_j + n_j) \quad . \quad (2.36)$$

Since  $n$  is completely uncorrelated, all linear terms involving the noise in (2.36) will average to zero. The mixed second order moment reduces to

$$M_{XY}[s(r)] = \frac{1}{N(r)} \sum_{P(r)} c_i c_j = M_{XY}[c(r)] \quad . \quad (2.37)$$

Since the average of the noise is zero, the average of the total signal equals the average of its coherent component, and the covariance equals

$$C[s(r)] = M_{XY}[s(r)] - M_X^2[s(r)] = C[c(r)] \quad . \quad (2.38)$$

The ordinary second moment reads

$$M_{XX}[s(r)] = \frac{1}{N(r)} \sum_{P(r)} s_i^2 = \frac{1}{N(r)} \sum_{P(r)} c_i^2 + 2c_i n_i + n_i^2 \quad . \quad (2.39)$$

<b>NWP SAF</b>	<b>On the quality of high resolution wind fields</b>	Doc ID : NWPSAF-KN-TR-002 Version : 1.2 Date : 31-08-2006
----------------	--	---

Because  $n$  is completely uncorrelated, the cross term will cancel in the averaging process, but the quadratic terms remain. As a consequence

$$M_{XX}[s(r)] = \frac{1}{N(r)} \sum_{P(r)} c_i^2 + n_i^2 = M_{XX}[c(r)] + M_{XX}[n(r)] \quad . \quad (2.40)$$

The variance therefore equals

$$\sigma^2[s(r)] = M_{XX}[s(r)] - M_X^2[s(r)] = \sigma^2[c(r)] + \sigma^2[n(r)] \quad . \quad (2.41)$$

Finally, the autocorrelation can be written as

$$\rho(r) = \frac{C[s(r)]}{\sigma^2[s(r)]} = \frac{C[c(r)]}{\sigma^2[c(r)] + \sigma^2[n(r)]} \quad . \quad (2.42)$$

At the origin,  $\rho(0) = 1$  by definition. However, when the distance approaches zero, the covariance approaches the variance, and (2.42) yields

$$\lim_{r \rightarrow 0} \rho(r) = \frac{\sigma^2[c(0)]}{\sigma^2[c(0)] + \sigma^2[n(0)]} = \frac{\sigma_c^2}{\sigma_c^2 + \sigma_n^2} \quad , \quad (2.43)$$

with  $\sigma_c$  and  $\sigma_n$  the standard deviation of the coherent signal and the noise, respectively. This shows that the autocorrelation will not be a continuous function at  $r = 0$ : when  $r$  decreases, the autocorrelation approaches the value  $1 - a$  rather than one, with

$$a = \frac{\sigma_n^2}{\sigma_c^2 + \sigma_n^2} = \frac{\sigma_n^2}{\sigma_s^2} \quad , \quad (2.44)$$

where  $\sigma_s$  is the standard deviation of the total signal. From this one arrives at

$$\sigma_n = \sigma_s \sqrt{a} \quad . \quad (2.45)$$

The standard deviation of the noise is therefore proportional to the square root of the size of the discontinuity in the autocorrelation at the origin. Figure 2.2 illustrates that this discontinuity leads to a constant noise floor in the spectrum.

## **2.4 The effect of a finite interval on the spectrum**

In section 2.2 the numerical implementation of the spectrum calculation was tested for a delta function and a Gaussian. In principle, the Fourier transform of a Gaussian is again a Gaussian, if the interval under consideration is infinite. In practice, the interval should be large enough to ascertain that both the function and its Fourier transform are small enough at the edges, while the

<b>NWP SAF</b>	<b>On the quality of high resolution wind fields</b>	Doc ID : NWPSAF-KN-TR-002 Version : 1.2 Date : 31-08-2006
----------------	--	---

sampling density should be large enough to reproduce the shape of the function. Figure 2.2 was obtained with  $a = (16\Delta)^{-2}$ , so at the edges  $r = \pm 128\Delta$  the function value equals  $e^{-64}$ , and the function drops off to  $e^{-1}$  over 16 points.

The exponential function is better suited to study the effects of a finite interval than the Gaussian, because all integrals can be done analytically. Suppose the simulated autocorrelation is given by

$$\rho_{sim}(x) = e^{-ax} \quad , \quad 0 \leq x \leq R_{max} \quad . \quad (2.46)$$

When symmetrized, as described in section 2.2, the function reads

$$\bar{\rho}_{sim}(x) = e^{-a|x|} \quad , \quad -R_{max} \leq x \leq R_{max} \quad . \quad (2.47)$$

In the limit that  $R_{max}$  approaches infinity, the Fourier transform of (2.51) is easily calculated as

$$\bar{R}_{sim}(k) = \int_{-\infty}^{\infty} dx e^{2\pi kx} e^{-a|x|} = \frac{2a}{a^2 + 4\pi^2 k^2} \quad , \quad (2.48)$$

with  $k = r^{-1}$  the spatial frequency and the overbar indicating that the function is defined on the symmetrized interval. The spectrum  $\Psi_{sim}$  is simply the square of  $\bar{R}_{sim}$ ,

$$\Psi_{sim}(k) = \frac{4a^2}{[a^2 + 4\pi^2 k^2]^2} \quad . \quad (2.49)$$

Note that the spectrum is continuous, despite the discontinuity in the derivative of the simulated autocorrelation at the origin.

Also for a finite interval, the spectrum is easily evaluated. The Fourier transform of the simulated autocorrelation reads

$$\bar{R}_{sim}(k) = \int_{-R_{max}}^{R_{max}} dx e^{2\pi kx} e^{-a|x|} \quad . \quad (2.50)$$

Some simple algebra yields

$$\bar{R}_{sim}(k) = \frac{2a}{a^2 + \beta^2} - \frac{2e^{-aR_{max}}}{a^2 + \beta^2} [a \cos(\beta R_{max}) - \beta \sin(\beta R_{max})] \quad , \quad (2.51)$$

with  $\beta = 2\pi k$ . The first term of (2.51) is the same as that of (2.48), while the second is an oscillating correction that vanishes exponentially with increasing  $R_{max}$ . When using a FFT algorithm, the Fourier transform is given at spatial frequencies

$$k_j = j\Delta k = \frac{j}{N_F \Delta} = \frac{j}{2R_{max}} \quad , \quad (2.52)$$

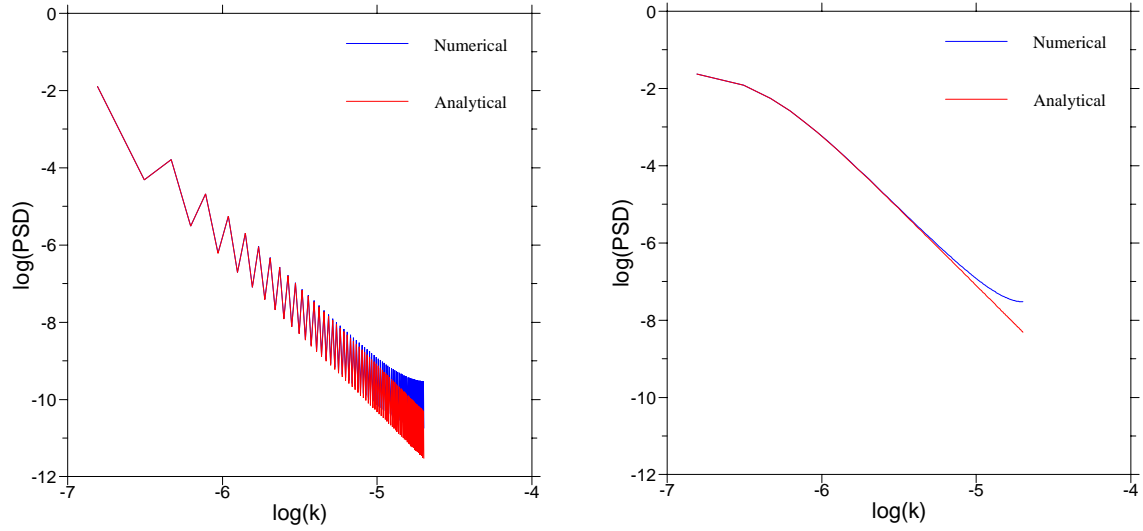


**Figure 2.3** Simulated spectra. Left:  $a = 2/R$ ; right  $a=16/R$ .

with  $j$  an integer and  $N_F$  the number of points in the interval. The arguments of the sine and cosine in (2.51) then reduce to  $j\pi$ , which yields zero for the sine and  $(-1)^j$  for the cosine. The Fourier transform is evaluated at the extremes of the oscillatory cosine contribution and will alternate.

Figure 2.3 shows the simulated spectrum for a small interval (left) and a large interval (right). The numerical results are indiscernible from the analytical results for spatial frequencies smaller than  $10^{-5}$ . For larger spatial frequencies the numerical spectrum tends to become more horizontal. This is most probably due to aliasing.

The oscillations in the spectrum can be filtered out by application of a window function [Press *et al.*, 1986]. A popular choice is the Hanning window given by

$$h(x) = 1 + \cos\left(\frac{\pi x}{R_{\max}}\right), \quad (2.53)$$

which equals zero for  $x = \pm R_{\max}$  and one for  $x = 0$ . Note that for an exponential simulated autocorrelation the spectrum can be obtained analytically also when filtered with this function. Writing the cosine in exponential form, the Fourier transform of the Hanning windowed exponential autocorrelation reads

<b>NWP SAF</b>	<b>On the quality of high resolution wind fields</b>	Doc ID : NWPSAF-KN-TR-002 Version : 1.2 Date : 31-08-2006
----------------	--	---

$$\bar{R}_{win}(k) = \int_{-R_{max}}^{R_{max}} dx e^{2\pi i k x} e^{-a|x|} \left[ 1 + \frac{1}{2} e^{\frac{i\pi x}{R_{max}}} + \frac{1}{2} e^{-\frac{i\pi x}{R_{max}}} \right]. \quad (2.54)$$

This can be rewritten as

$$\bar{R}_{win}(k) = \bar{R}_{sim}(k) + \frac{1}{2} \int_{-R_{max}}^{R_{max}} dx e^{2\pi i k x} e^{-a|x|} \left[ e^{\frac{i\pi x}{R_{max}}} + e^{-\frac{i\pi x}{R_{max}}} \right]. \quad (2.55)$$

Some simple algebra yields

$$\begin{aligned} \bar{R}_{win}(k) = & \frac{2a}{a^2 + \beta^2} - \frac{2e^{-aR_{max}}}{a^2 + \beta^2} [a \cos(\beta R_{max}) - \beta \sin(\beta R_{max})] + \\ & + \frac{a}{a^2 + \beta_+^2} + \frac{e^{-aR_{max}}}{a^2 + \beta_+^2} [a \cos(\beta R_{max}) + \beta_+ \sin(\beta R_{max})] + \\ & + \frac{a}{a^2 + \beta_-^2} + \frac{e^{-aR_{max}}}{a^2 + \beta_-^2} [a \cos(\beta R_{max}) + \beta_- \sin(\beta R_{max})], \end{aligned} \quad (2.56)$$

where  $\beta_{\pm} = \beta \pm \pi / R_{max}$  and  $\beta = 2\pi k$ .

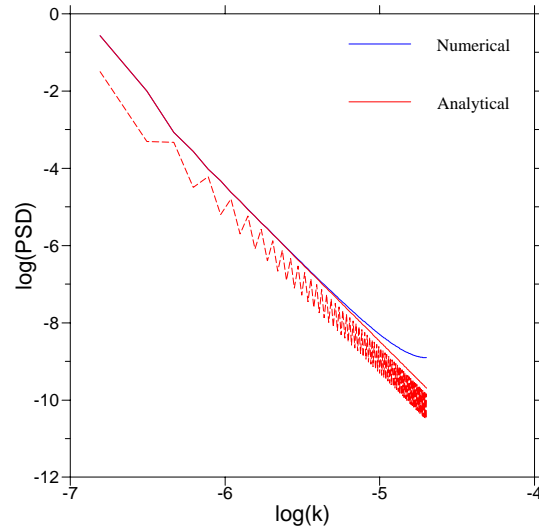


**Figure 2.4** Numerical and analytical spectrum for the exponential simulated autocorrelation with Hanning window (solid curves) and the analytical spectrum without window (dashed curve).

<b>NWP SAF</b>	<b>On the quality of high resolution wind fields</b>	Doc ID : NWPSAF-KN-TR-002 Version : 1.2 Date : 31-08-2006
----------------	--	---

Figure 2.4 shows the resulting spectra, with the analytical spectrum without window, (2.51) shown as a reference (dashed red curve). Application of the Hanning window removes the oscillations. The first and second term of (2.56) are identical to (2.51). At the FFT grid point  $k_j$  the sines in (2.56) equal zero and the cosines equal  $(-)^j$ . The alternating cosine contribution is now for a large part (but not completely) eliminated by the extra terms. However, in between the FFT grid points, the oscillations remain (no results shown). The numerical result agrees well with the analytical expression, except at high spatial frequencies where aliasing causes some difference.

The Hanning window does not change the range of the autocorrelation function. It remains between -1 and +1 (or, more specific, between -0.4 and +1 in the study presented here). However, it does change the gradient of the autocorrelation function by amplifying negative slopes. As illustrated in figure 2.3, steeper slopes in the autocorrelation lead to higher amplitudes in the spectral density..

It is concluded that one must therefore be careful in interpreting the spectrum when it tends to become horizontal at high frequencies. It may be due to uncorrelated noise, as in figure 2.2, but it may also be a numerical effect as in figures 2.3 and 2.4. Moreover, window functions generally affect the amplitude of the spectral density, thereby weakening the link to the underlying physical problem under investigation. The autocorrelation is better suited for estimating the noise and small-scale properties of the scatterometer wind fields investigated here.

NWP SAF	<b>On the quality of high resolution wind fields</b>	Doc ID : NWPSAF-KN-TR-002 Version : 1.2 Date : 31-08-2006
---------	--	---

## 3 Results for the autocorrelation

This chapter contains the results for the autocorrelations obtained for one month of SeaWinds data. A standard result is defined in section 3.2. This standard result is used as a reference for studying the effects of geographical zone, wind vector cell number along the swath, orbit section, and solution scheme. Special attention is paid to the behaviour of the autocorrelation at short distances.

### 3.1 *The SeaWinds data set*

The results shown in this section were obtained from all SeaWinds data recorded in December 2004 that were available in KNMI's MOS archive (872 files). The SeaWinds data are stored in half-orbit files with multiple BUFR messages. Each BUFR message contains one line of wind vector data perpendicular to the satellite direction. At 25 km resolution there are 76 individual wind vector cells.

The dataset from the MOS archive is not complete: five gaps were found, measuring 1062, 603, 1, 1033, and 1063 lines, respectively. The gap of size 1 is due to a wrong BUFR message, the other gaps are due to missing files.

There is an overlap between consecutive files of at least 140 lines (3500 km). However, due to the observation strategy of SeaWinds, a semicircle of data is lacking for each file at the start (because the backward looking radar observations are not included) and at the end (because the forward looking radar observations are not included). The first file is read and processed from the start to 40 BUFR messages from the end (at 25 km resolution), to avoid the semicircle of missing data. Processing of the second and following files is resumed when a new line number is encountered. Due to the overlap, this is well beyond the semicircle of missing data at the start of each file. Processing is stopped 40 messages from the end of the file.

This ensures an overlapping dataset. Only when a gap is encountered, the semicircle of data at the end of the last file before the gap is ignored. As this happens only four times for 872 files, this will have no effects on the results.

Wind vectors are rejected if either the KNMI-JPL rain flag is set, or if the variational ambiguity removal (2DVAR) quality control flag is set.

<b>NWP SAF</b>	<b>On the quality of high resolution wind fields</b>	Doc ID : NWPSAF-KN-TR-002 Version : 1.2 Date : 31-08-2006
----------------	--	---

Results will be presented for the zonal and meridional wind components,  $u$  and  $v$ , respectively, as well for the wind component perpendicular and parallel to the satellite moving direction,  $P$  and  $T$ , defined as

$$\begin{aligned} P &= u \cos \alpha + v \sin \alpha \\ T &= -u \sin \alpha + v \cos \alpha \end{aligned} \quad (3.1)$$

where  $\alpha$  is the satellite heading, i.e., the angle between the satellite moving direction and the local meridian measured counterclockwise from the north. The autocorrelations of the wind components  $P$  and  $T$  may offer information on the two-dimensional variational ambiguity removal (2DVAR) scheme.

The satellite heading is given in the NOAA BUFR messages, but not for every row and with a precision of  $1^\circ$ . Therefore  $\alpha$  is calculated from the positions of the WVC's. These are given up to  $0.1^\circ$ , which may lead to an error up to 3 km in the distance between adjacent WVC's when calculated from these positions. To minimize errors, the calculation of  $\alpha$  is based on the positions of the first and last WVC. The differences in latitude and longitude are transformed to distances in  $x$  and  $y$  on a plane, correcting for the fact that the relation between distance and difference in longitude depends on the cosine of the latitude, for which the average latitude is taken.

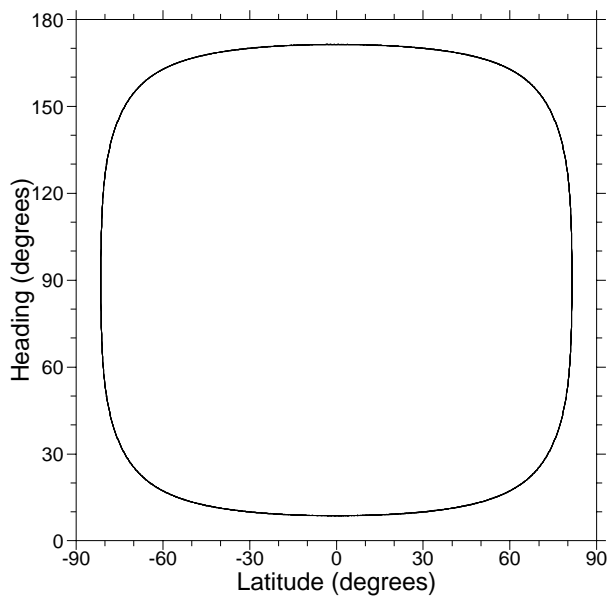


**Figure 3.1.** QuikSCAT heading as a function of latitude.

NWP SAF	<b>On the quality of high resolution wind fields</b>	Doc ID : NWPSAF-KN-TR-002 Version : 1.2 Date : 31-08-2006
---------	--	---

Figure 3.1 shows the satellite heading as a function of latitude. When QuikSCAT passes the equator from south to north (ascending pass), the heading is small, 8.7°. The heading slowly increases and goes rapidly through 90° when QuikSCAT reaches the most northern point of its orbit. The wind vector cells are then aligned along a meridian from south to north. The heading reaches its maximum value of about 171.3° when QuikSCAT passes the equator from north to south (descending pass). When QuikSCAT reaches its most southern point of its orbit, the heading is 90° and the WVC's are again oriented along a meridian from south to north.

### 3.2 Standard results

In order to simplify comparison, a standard result has been defined. It is obtained from the SDP processed data of December 2004 at 25 km resolution without Multiple Solution Scheme. Figure 3.2 shows the results for the zonal (west-east) and meridional (north-south) wind components  $u$  and  $v$ , for the SDP scatterometer winds and the model results from the NCEP model. Figure 3.2 shows the autocorrelation for each WVC in grey, and the average over all WVC's in black.

Figure 3.2 shows that two WVC's behave very different from the others, especially for  $u$ . These cells are the outermost WVC's containing data, numbers 9 and 67. Due to irregularities in the SeaWinds orbit these cells are not always filled with radar observations. Their statistics therefore differ from that of the other cells due to sampling differences (see also section 3.3).

When the distance decreases to zero, the autocorrelations of the model winds approach 1 smoothly, apparently with zero derivatives. The autocorrelation of the scatterometer winds, on the other hand, approach a value slightly lower than 1 with nonzero derivative. As shown in section 2.3, this may be due to noise in the scatterometer winds. The model winds are much smoother and don't show this effect. Another striking fact in figure 3.2 is that the autocorrelations become negative for large distances, notably for  $u$  at distances larger than 2000 km and less clearly for  $v$  at distances exceeding 2500 km. It will be shown in section 3.3 that this reflects the large scale structure of the Earth's wind field.

Figure 3.3 is similar to figure 3.2, but now for the wind components perpendicular and parallel to the satellite direction,  $P$  and  $T$ , respectively. The autocorrelations of  $P$  and  $T$  behave similar to those of  $u$  and  $v$ .

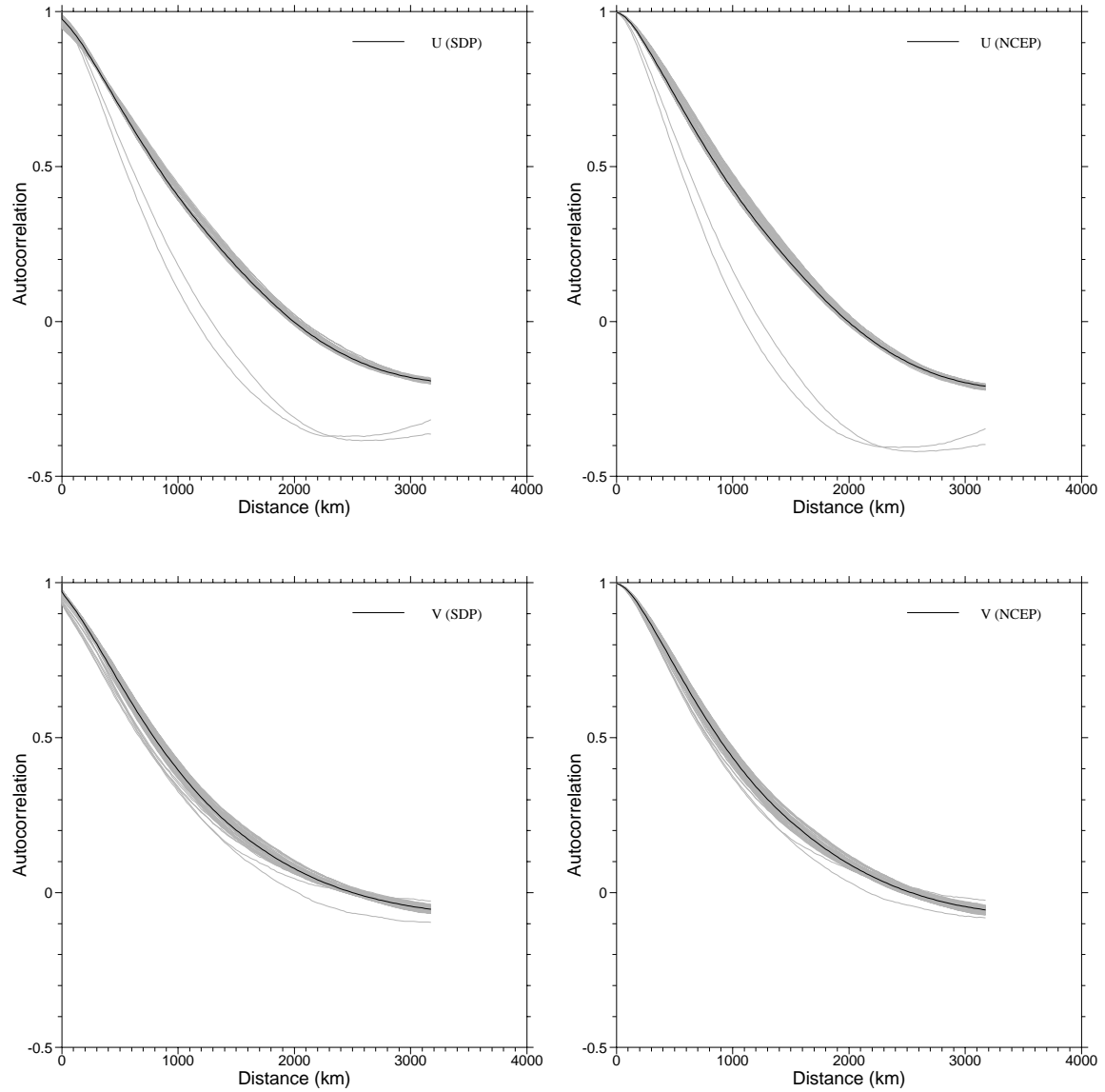


**Figure 3.2** Autocorrelation as a function of distance for the SDP retrieved winds (left) and the NCEP model calculations (right). Top: zonal wind component  $u$ , bottom: meridional wind component  $v$ .

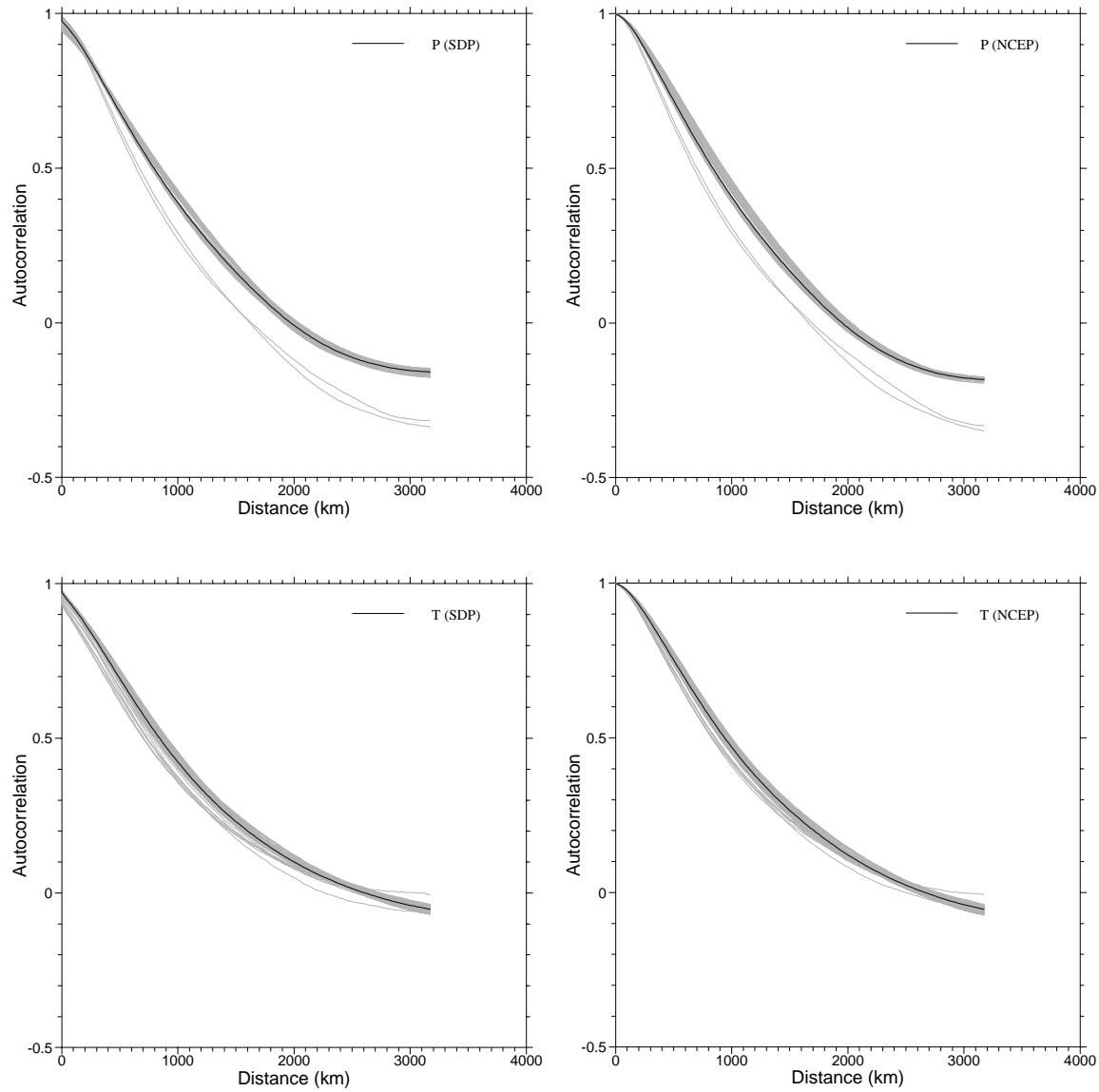


**Figure 3.3** Autocorrelation as a function of distance for the SDP retrieved winds (left) and the NCEP model calculations (right). Top: perpendicular wind component *P*, bottom: parallel wind component *T*.

NWP SAF	<b>On the quality of high resolution wind fields</b>	Doc ID : NWPSAF-KN-TR-002 Version : 1.2 Date : 31-08-2006
---------	--	---

### 3.3 Geographical zone, WVC, and orbit

Figure 3.4 shows the effect of the geographical zone and the WVC on the autocorrelation as a function of distance. The black curves are for the whole Earth, while the red curves are restricted to the tropics, latitude within the interval  $[-30^\circ, +30^\circ]$  and the blue curves to the extratropics, latitude outside  $[-30^\circ, +30^\circ]$ . The dashed curves are averaged over nodes 11-30 (left sweet swath), the solid curves over nodes 31-46 (nadir swath), and the dotted curves over nodes 47-66 (right sweet swath).

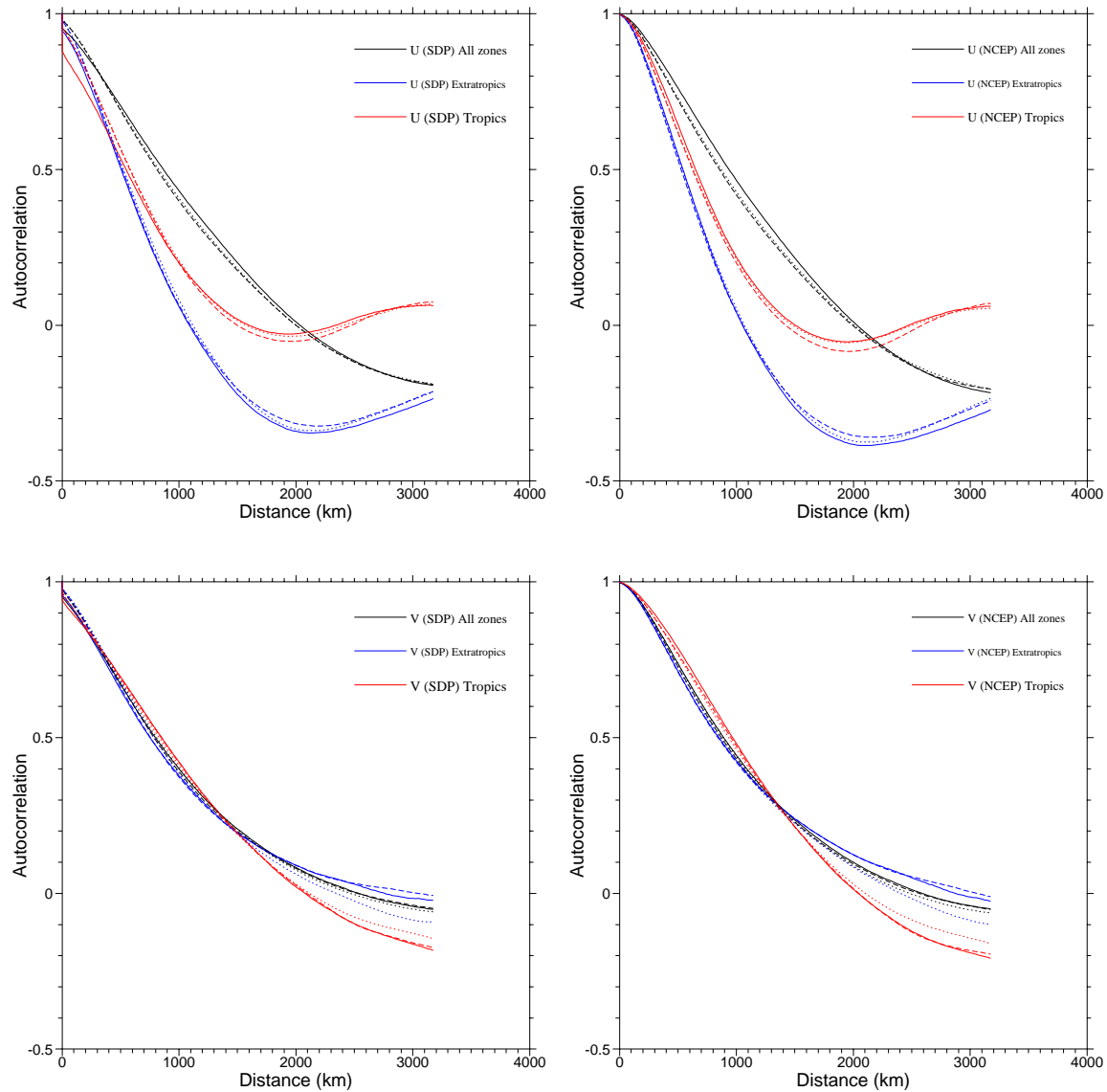
Figure 3.4 shows that the WVC range chosen has less impact on the autocorrelation than the geographical zone, and that the autocorrelation of the scatterometer winds behave similar to that of the model winds. Note that the curves for the tropics and those for the extratropics are not each others complement, because both points of the lag should lie in the zone specified. Therefore a band around  $-30^\circ$  and one around  $+30^\circ$  is excluded, because the lag points lie in different zones. Notably for large lag distances, this band has an appreciable width, and the autocorrelations for the whole Earth (black curves) differ significantly from those for the tropics and the extratropics (red and blue curves).

Comparison of figure 3.4 with figure 3.2 shows that the wind vectors contributing to the autocorrelation of WVC 9 and 67 originate from the extratropics. Indeed, there are few contributing pairs in the tropics.

The autocorrelation of the zonal wind component,  $u$ , varies strongly with the geographical zone. When averaged over the whole Earth, the autocorrelation becomes slightly negative for distances larger than about 2000 km. In the extratropics the autocorrelation becomes zero at smaller distances of the order of 1000 km. The maximum anticorrelation is reached for distances of about 2000 km, and for larger distances the correlation increases again. The correlation for the tropics is around zero for distances of the order of 2000 km and increases to small positive values for larger distances.

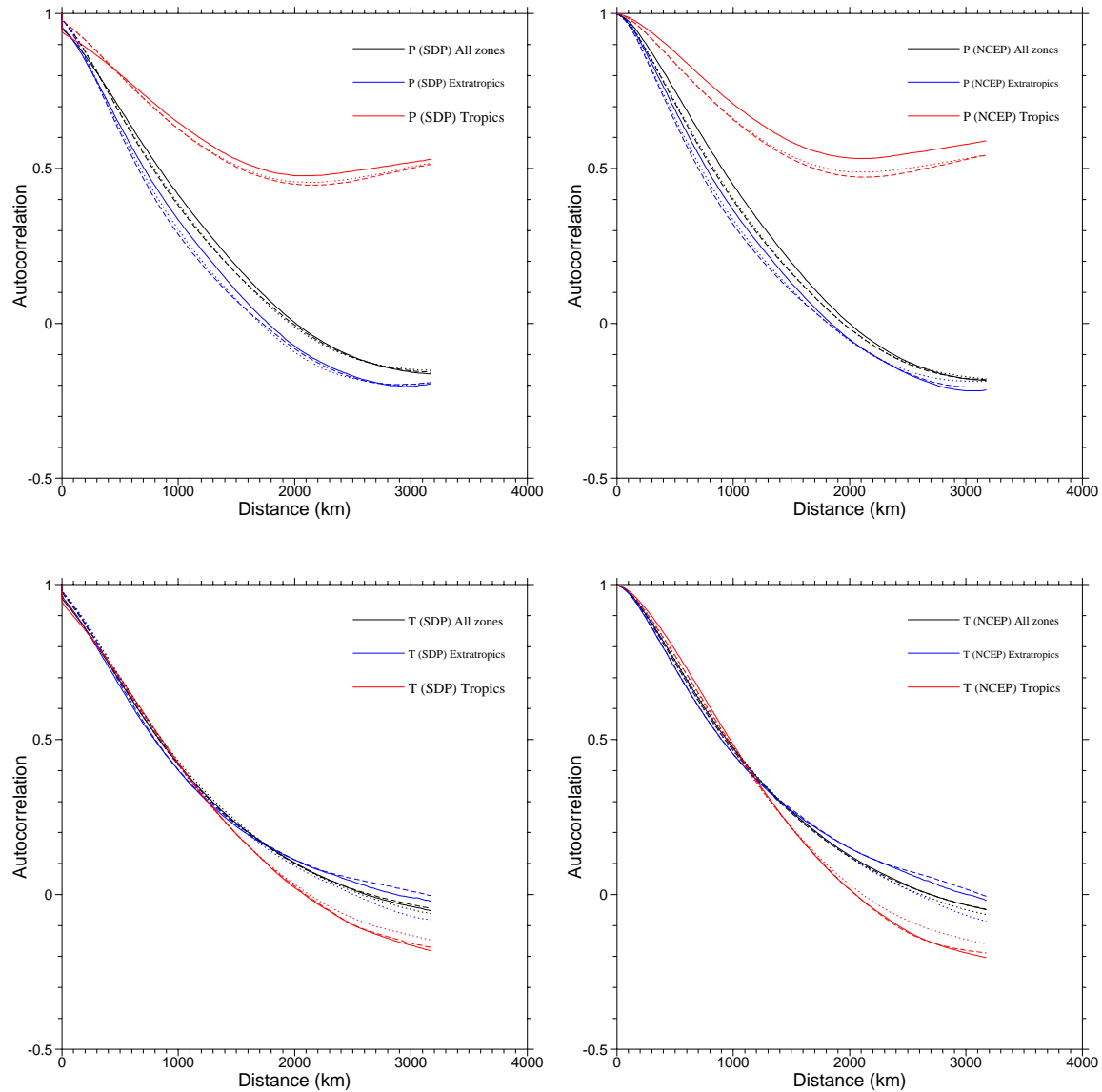
The autocorrelation in the meridional component,  $v$ , shows less structure than that in  $u$ . The autocorrelation gradually decreases monotonically to values around or slightly below zero at large distances.

Figure 3.5 is similar to figure 3.4, but now for the wind components perpendicular and parallel to the satellite moving direction,  $P$  and  $T$ , respectively. The autocorrelation of  $P$  for the tropics stays positive and rather large: 0.5 or more, for both the scatterometer wind and the model wind. The autocorrelation of  $P$  for the extratropics resembles that for the whole Earth. The autocorrelations in  $T$  show less variation with geographical zone.



**Figure 3.4** Autocorrelation versus distance for various geographical zones and WVC ranges. Black curves: all Earth; blue curves: extratropics, and red curves: tropics. Dashed curves: WVC 11-30 (sweet swath); solid curves: WVC 31-46 (nadir swath); dotted curves: WVC 47-66 (sweet swath). Upper panels: zonal component  $u$ ; lower panels: meridional component  $v$ . Left panels: scatterometer winds; right panels: model winds.

It is rather surprising that the autocorrelation of  $P$  in the tropics differs so much from that of  $u$ , because the satellite heading shows little variation for geographical latitudes between  $-30^\circ$  and  $+30^\circ$ , see figure 3.1. For ascending passes  $P$  and  $u$  are roughly parallel, and for descending passes they are roughly antiparallel.



**Figure 3.5** As figure 3.4, but now for the wind components perpendicular (upper panels) and parallel (lower panels) to the satellite direction.

Figure 3.6 shows the contributions to the autocorrelation in the scatterometer  $u$  (left) and  $P$  (right) for the tropics from the ascending and descending passes (dashed and dotted curves, respectively). The solid curves are for all passes and are identical to the corresponding curves in figures 3.4 and 3.5.

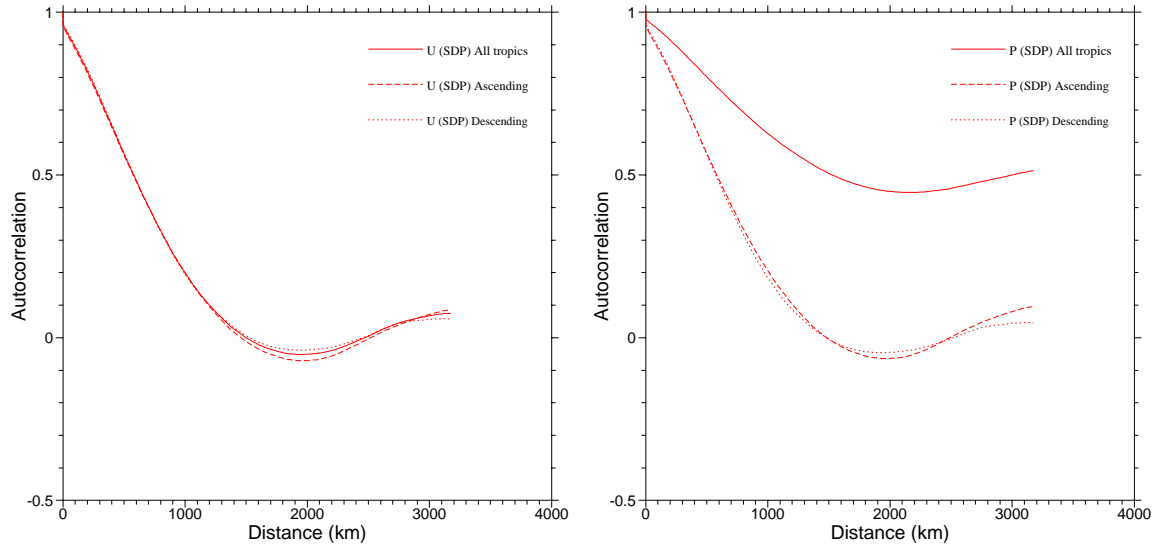


**Figure 3.6** Autocorrelation in the tropics for the scatterometer wind components  $u$  (left) and  $P$  (right). Solid: both ascending and descending orbits; dashed: only ascending orbits; dotted: only descending orbits.

All curves in figure 3.6 are averages over WVC 11 to 66, since figures 3.5 shows that the swath has little influence compared to that of the geographical zone. Figure 3.6 shows that the contributions of the ascending and descending passes to the autocorrelations of  $u$  and  $P$  differ little from each other, as expected. However, when taken together for all passes (and indeed the contributions from each pass is independent, as there is no overlap of data between the passes in the tropics), the autocorrelation of  $P$  becomes strongly positive. Since the orientation of  $P$  changes almost  $180^\circ$  for ascending and descending passes, some interference in the moments must cause this behavior.

Figure 3.7 shows the first and second moments of the scatterometer wind components  $u$  (left) and  $P$  (right) in the tropics. The contributions of ascending and descending orbits are plotted separately (dashed and dotted curves, respectively) and together (solid curves). The curves are averaged over WVC 11 to 66.

The first moment  $M_x$  of the perpendicular wind component  $P$  varies quite strongly with the orbit. It is positive with a value around +4 m/s for ascending passes and negative with a value around -4 m/s for negative values. It vanishes when ascending and descending orbits are combined. Note that the first moment of  $u$  is always negative around -4 in figure 3.7. The second moment  $M_{xx}$  varies little with distance and has a value around  $30 \text{ m}^2/\text{s}^2$ , for both  $u$  and  $P$ . The mixed second order moment  $M_{xy}$  decreases and has a minimum value around  $16 \text{ m}^2/\text{s}^2$  at a distance between 2000 and 2500 km.

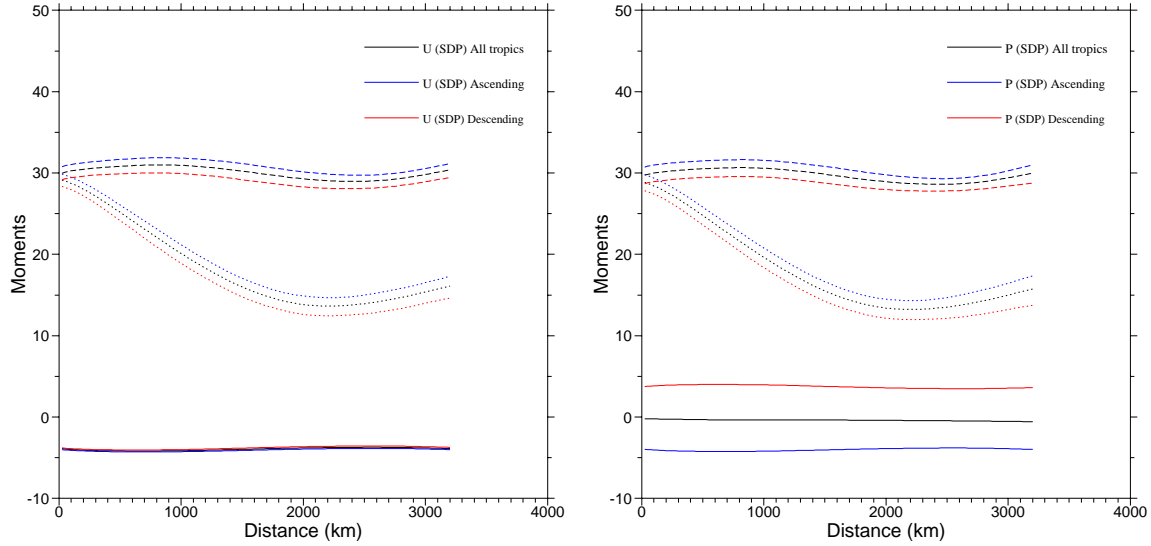


**Figure 3.7** First and second moments for  $u$  (left) and  $P$  (right). Solid: first moment  $M_X$ ; dashed: second moment  $M_{XX}$ ; dotted: mixed second moment  $M_{XY}$ . Black: both ascending and descending orbits; blue: only ascending orbits; red: only descending orbits.

When  $M_X$  vanishes, as for the black curve in the right panel of figure 3.7, the autocorrelation (2.15) reduces to the quotient of  $M_{XX}$  and  $M_{XY}$ , which is around 0.5 for large distances. If  $M_X$  equals  $\pm 4$  m/s, it contributes significantly to the covariance (2.18). In fact, it cancels the contribution of the mixed second order moment at large distances, so the covariance, and hence the autocorrelation becomes small.

So the different behavior of the autocorrelations of  $u$  and  $P$  in the tropics is caused by differences in the average wind speed. Around the equator, the wind field is dominated by trade winds which are southeast north of the equator and northeast south of the equator. Therefore  $u$  is negative both north and south of the equator, leading to an average value of  $u$  of about -4 m/s. This cancels the covariance, which is rather high at large distances due to the trades, leading to a small autocorrelation. Since the orientation of  $P$  differs  $164^\circ$  between ascending and descending passes, the dominating contributions of the trades cancel each other. The average of  $P$  is small, but since the mixed second order moment  $M_{XY}$  is about half the second moment  $M_{XX}$ , the covariance at large distances is large. However, this does not represent flow changes relative to the Earth reference frame and therefore provides no useful guidance with respect to the tropical flow.

### 3.4 Multi Solution Scheme (MSS)

SDP can use the Multiple Solution Scheme (MSS) for ambiguity removal [SCAT group, 2006]. In this scheme, up to 144 wind vector solutions with their probability are identified and fed into the Ambiguity Removal step. The MSS is able to select solutions that are not exactly at the minimum value of the MLE but represent the wind field better, in contrast to traditional methods which are restricted to solutions at the MLE minima.

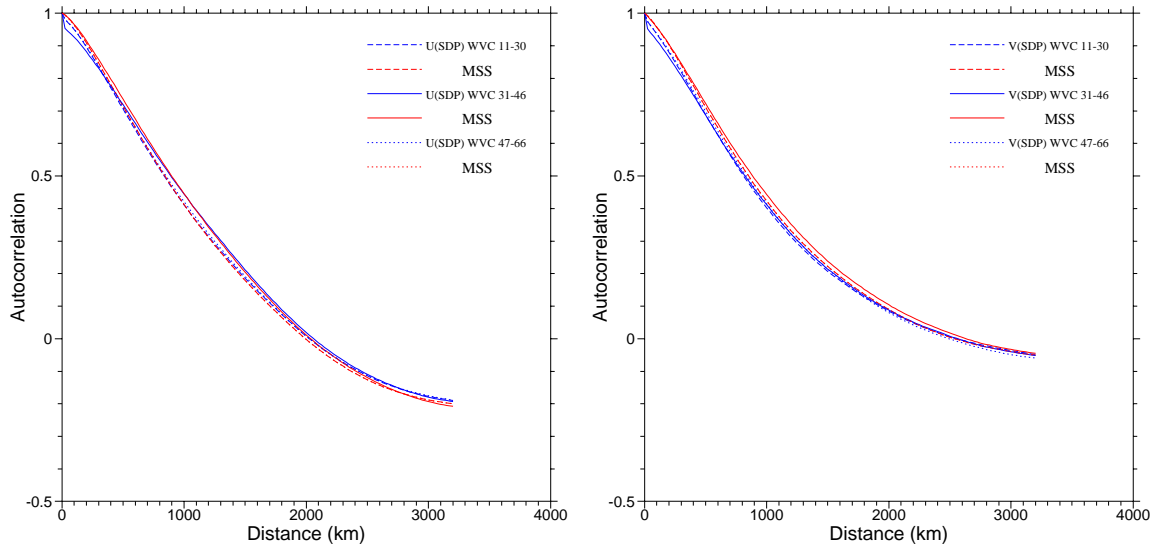


**Figure 3.8** Autocorrelation of the wind speed components  $u$  (left) and  $v$  (right) for the left sweet swath (dashed curves), the nadir swath (solid curves), and the right sweet swath (dotted curves). The black curves are for the standard SDP run, the blue curves are obtained using the MSS.

Figure 3.8 shows the results for the autocorrelation of  $u$  and  $v$  averaged over the three swath regions (left sweet, nadir, and right sweet). The standard SDP run (black curves) shows that the nadir swath (solid curves) has a higher noise peak at the origin than the sweet swaths (dashed and dotted curves). When using the MSS (blue curves), the noise peak becomes much smaller, indicating that use of the MSS indeed results in a less noisy wind field.

<b>NWP SAF</b>	<b>On the quality of high resolution wind fields</b>	Doc ID : NWPSAF-KN-TR-002 Version : 1.2 Date : 31-08-2006
----------------	--	---

NWP SAF	<b>On the quality of high resolution wind fields</b>	Doc ID : NWPSAF-KN-TR-002 Version : 1.2 Date : 31-08-2006
---------	--	---

## 4 Quantification of the noise level

### 4.1 Estimation of the noise peak height

The differences between the autocorrelations from the scatterometer winds and those from the model winds are small in figures 3.4 and 3.5. Only at short distances the scatterometer winds show a discontinuity, whereas the model winds seem to approach zero continuously with zero derivative. This can be more clearly seen in figure 4.1, which shows the short distance parts of figures 3.4 and 3.5 for the scatterometer winds in more detail.

The discontinuity in the origin is a measure for the noise in the scatterometer wind field, because it is completely uncorrelated except for zero distance. In section 2.3 it was shown that the height of the discontinuity in the autocorrelation,  $a$ , is directly proportional to the noise variance  $\sigma_n^2$ . The constant of proportionality equals the total variance of the wind field,  $\sigma_s^2$ . In terms of standard deviations the relation reads  $\sigma_n = \sigma_s \sqrt{a}$  (equation 2.49).

From figure 4.1 it can be inferred that the noise component is larger for the autocorrelation in the tropics compared to those in the extratropics and over the whole Earth. One important reason is the abundance in rainfall around the equator which disturbs the scatterometer signal and leads to lower quality wind estimates. Another cause is the fact that the wind speeds in the tropics are on average smaller than in the extratropics, leading to higher signal-to-noise ratios. The noise is also larger in the nadir swath than in the sweet swaths. This is because the observation geometry in the nadir swath is less favorable for wind estimation than in the sweet swaths.

In order to quantify the noise level, the height of the discontinuity in the autocorrelation at the origin must be estimated. The following procedures have been compared:

- Interpolation of the symmetrized autocorrelation at the origin using smoothing splines [Woltring, 1986].
- Extrapolation of the non-symmetrized autocorrelation to the origin using
  - A linear function fitted to the first two autocorrelations  $\rho(\Delta)$  and  $\rho(2\Delta)$ ;
  - A quadratic function fitted to the first three autocorrelations  $\rho(\Delta)$ ,  $\rho(2\Delta)$ , and  $\rho(3\Delta)$ ;
  - An exponential function fitted to the first two autocorrelations  $\rho(\Delta)$  and  $\rho(2\Delta)$ ;
  - A Gaussian function fitted to the first two autocorrelations  $\rho(\Delta)$  and  $\rho(2\Delta)$ ;
  - The product of an exponential function and a Gaussian function fitted to the first three autocorrelations  $\rho(\Delta)$ ,  $\rho(2\Delta)$ , and  $\rho(3\Delta)$ .

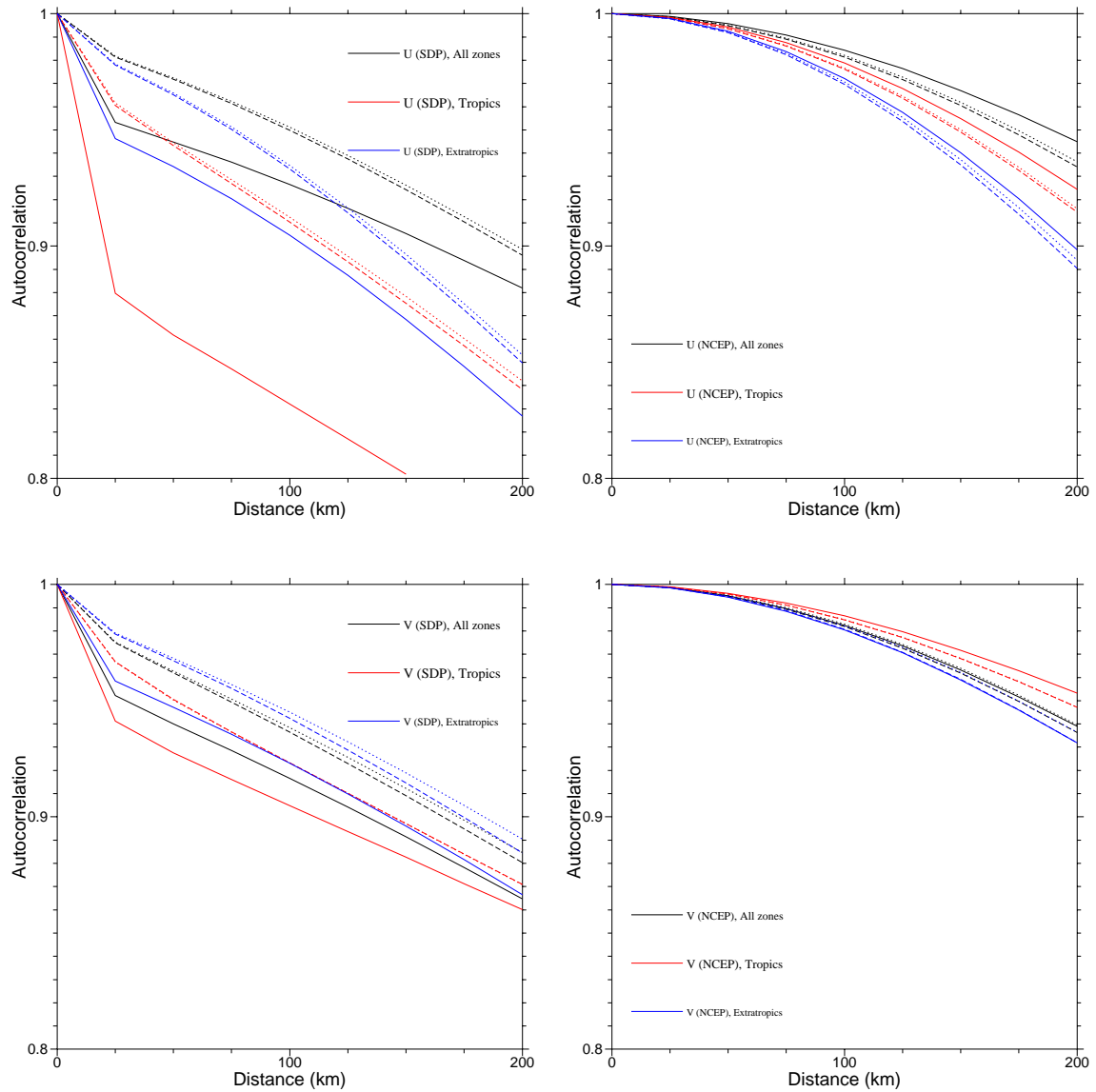


**Figure 4.1** Autocorrelation at short distances from the scatterometer winds. Dashed curves: averaged over WVC 11-30 (sweet swath); solid curves: averaged over WVC 31-46 (nadir swath); dotted curves: averaged over WVC 47-66 (sweet swath). Black curves: whole Earth; blue curves: extratropics; red curves: tropics. Left: scatterometer winds; right: model winds; upper: zonal component  $u$ ; lower: meridional component  $v$ .

Figure 4.2 shows the autocorrelation at short distance for the scatterometer wind speed components  $u$  and  $v$  after the discontinuity at the origin has been removed. The autocorrelation has been averaged over WVC's 11 to 66. The black curve shows the original autocorrelation which equals 1 at zero lag by definition.

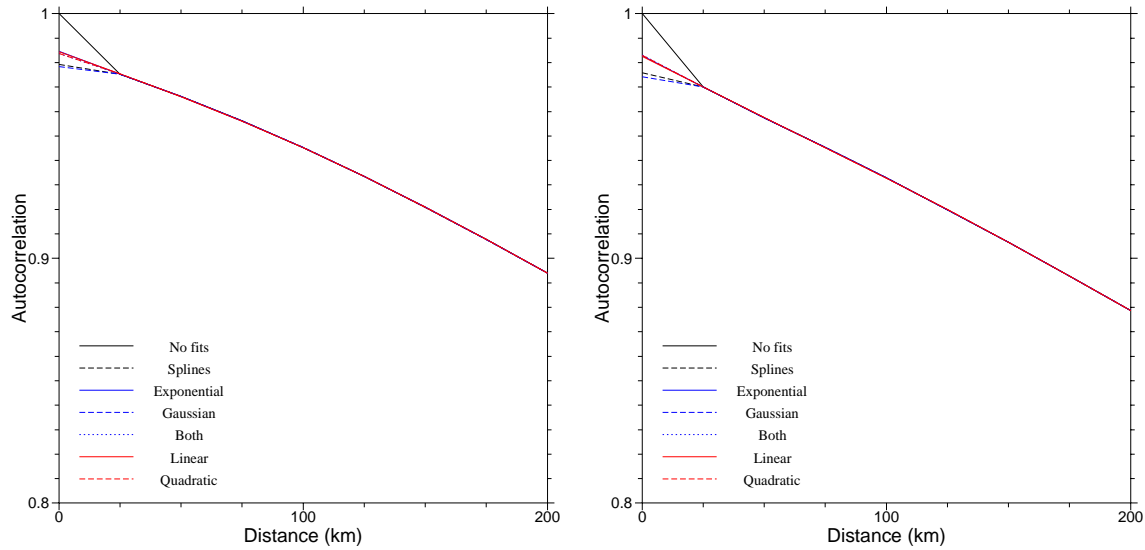


**Figure 4.2** The autocorrelation near the origin for the SDP wind speed components  $u$  (left) and  $v$  (right) after the noise peak has been removed using the various techniques discussed in the text.

Estimation of the noise peak height using smoothing splines or a Gaussian fit (dashed curves) impose zero derivative of the fitted autocorrelation at the origin. This is not realistic, and the noise peak height is overestimated. The other procedures differ little from each other, but quadratic extrapolation and the product of an exponential and a Gaussian produce the best continuous fit. Due to its simplicity quadratic extrapolation is therefore preferred for estimating the noise peak height.

Figure 4.3 shows the noise peak height as a function of WVC number for the scatterometer wind components  $u$  and  $v$  obtained with the various methods. The noise peak height is lowest for the sweet swaths and highest at nadir. Note that the noise peak height for  $u$  has a local minimum at nadir.

Interpolation with smoothing splines or extrapolation with a Gaussian give the highest values for the noise peak height, for the reasons mentioned above. The other methods show little difference, as expected

When applied to the model winds, the methods for estimating the noise peak do not produce significant values. The resulting noise peak heights are very small (of the order of  $10^{-4}$ ) and may even become negative. This is caused by statistical noise in the autocorrelations, which also causes the noise in the curves of figure 4.3.

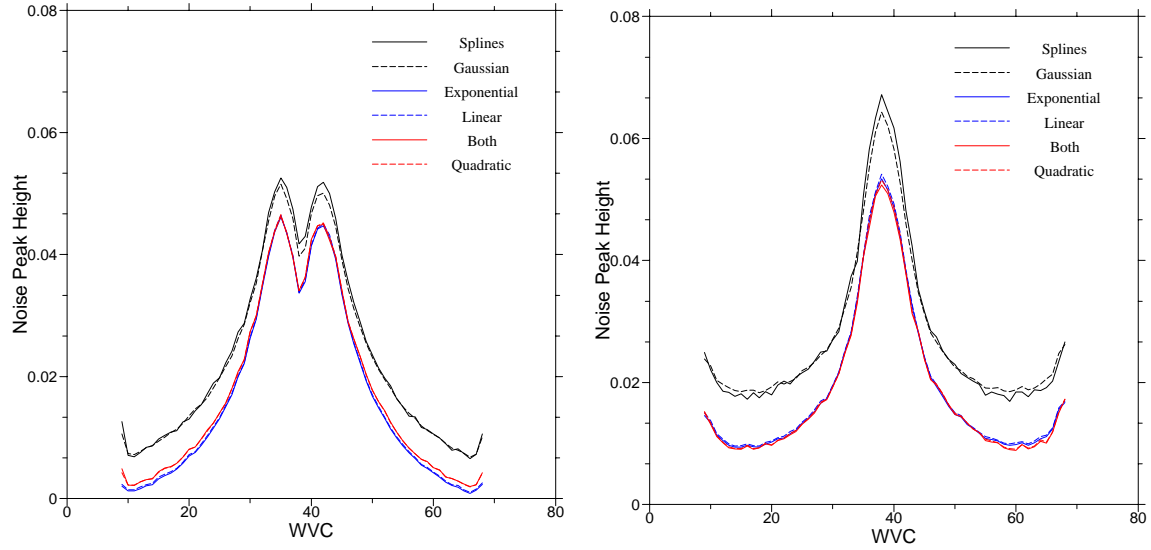


**Figure 4.3** Noise peak height as a function of WVC number for the scatterometer wind components  $u$  (left) and  $v$  (right) obtained with various methods as discussed in the text.

The previous discussion indicates that the error in the noise peak estimate consists of two components: a systematic one and a stochastic one. The systematic error depends on the extrapolation method chosen. For example, figure 4.2 shows that a Gaussian extrapolation tends to yield a higher value for the noise peak than the linear or quadratic extrapolation. The stochastic error can be estimated by fitting the autocorrelation with smoothing splines [Woltring, 1986] after removal of the noise peak at the origin with quadratic extrapolation. The mean squared residual of the fit is of the order of  $10^{-7}$ . It is therefore reasonable to adapt the square root of this value for  $\Delta\rho$ , the absolute error in the autocorrelation due to statistical noise, so  $\Delta\rho \approx 0.0003$ .

As illustrated in figure 4.2, a quadratic extrapolation gives good results. Assuming it is perfect, and writing  $\rho_i = \rho(x_i) = \rho(i\Delta)$ ,  $i = 0, \dots, N$ , it reads

$$\rho_0 = 1 - 3\rho_1 + 3\rho_2 - \rho_3 = 1 - a \quad , \quad (4.1)$$

with  $a$  the noise peak height. If the errors in the  $\rho_i$  are random and uncorrelated, the error in  $a$  for quadratic extrapolation is  $\sqrt{3^2 + 3^2 + 1} \approx 4.4$  times the error in the autocorrelation, so  $\Delta a \approx 0.0013$ . Note that this is consistent with the values of the order of  $10^{-4}$  found for the noise peak height in the model winds mentioned above. The total variance of the wind field is between 20 and 30. Therefore the error in the noise variance equals  $\Delta V_n \approx 0.03 \text{ m}^2/\text{s}^2$ . The error in the standard deviation of the noise,  $\Delta\sigma_n$ , can be obtained from

<b>NWP SAF</b>	<b>On the quality of high resolution wind fields</b>	Doc ID : NWPSAF-KN-TR-002 Version : 1.2 Date : 31-08-2006
----------------	--	---

$$\sigma_n \pm \Delta\sigma_n = \sqrt{V_n \pm \Delta V_n} \approx \sqrt{V_n} \left( 1 \pm \frac{\Delta V_n}{2\sqrt{V_n}} \right) = \sqrt{V_n} \pm \frac{1}{2} \Delta V_n \quad . \quad (4.2)$$

With  $\Delta V_n \approx 0.03 \text{ m}^2/\text{s}^2$  this yields  $\sigma_n \approx 0.015 \text{ m/s}$ . Small values of the noise variance,  $V_n \leq \Delta V_n$ , and small values of its standard deviation,  $\sigma_n \leq \Delta\sigma_n$ , are therefore not significant.

## 4.2 Standard results

Figure 4.4 shows the standard deviation of the noise level (in m/s) as a function of WVC number. The left panel shows the components  $u$  and  $v$ ; the right panel the components  $P$  and  $T$ .

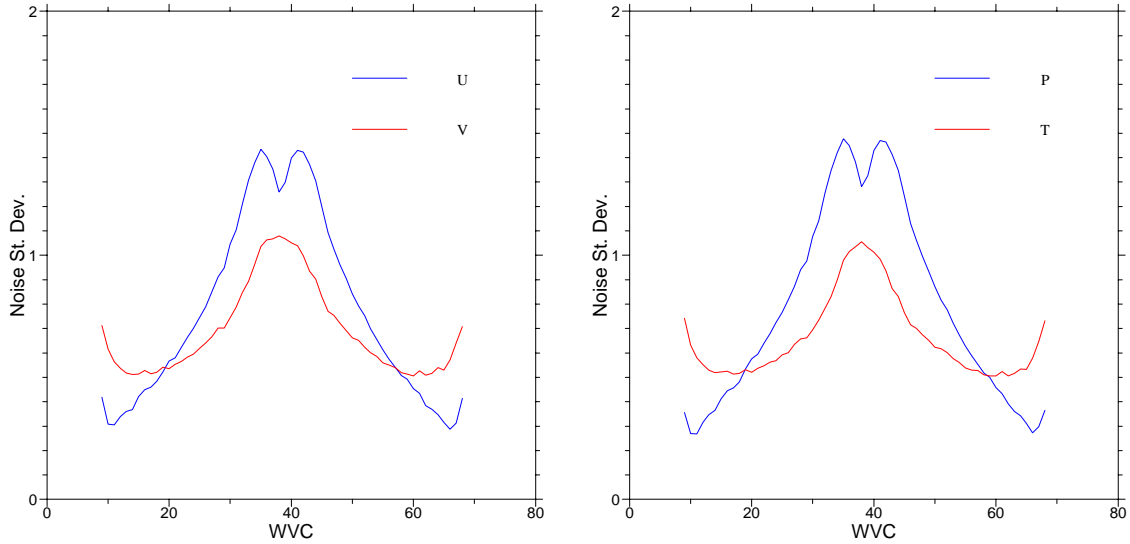


**Figure 4.4** Standard deviation of the noise level in the standard calculation for the components  $u$  and  $v$  (left) and for the components  $P$  and  $T$  (right).

Figure 4.4 shows little difference between  $u$  and  $P$  and between  $v$  and  $T$ , respectively. The noise contribution is lowest for the sweet parts of the swath, WVC 11-30 and 47-66, and highest in the nadir part of the swath, WVC 31-46. The noise level in  $u$  for WVC numbers smaller than 20 or higher than 50 is lower than that in  $v$ , but for WVC numbers between 20 and 50 the situation is reversed. The highest noise level exceeds 1.4 m/s in  $u$  and 1 m/s in  $v$ . This is a considerable contribution and causes the noisy appearance of the SDP retrieved wind fields, especially at nadir.

<p style="text-align: center;"><b>NWP SAF</b></p>	<p style="text-align: center;"><b>On the quality of high resolution wind fields</b></p>	<p>Doc ID : NWPSAF-KN-TR-002  Version : 1.2  Date : 31-08-2006</p>
---	---	--

The curves are not perfectly smooth. They contain some noise at a level consistent with an error in the standard deviation of the noise level of about 0.015 m/s as estimated in section 4.1.

### 4.3 Orbit and geographical zone

Figure 4.5 shows the standard deviation of the noise level in the SDP retrieved wind speeds for different parts of the orbit (left) and for different geographical zones (right). These have little influence. The noise level in  $u$  is slightly asymmetric for ascending and descending orbits, but this asymmetry averages out when all orbits are taken into account. The noise level in the tropics is generally slightly lower than that in the extratropics. Note that the curves in the right panel of figure 4.5 become noisy, especially those for  $v$ . This is because the autocorrelation is based on less lags. The autocorrelation contains more statistical noise and the estimation of the noise peak height gets less reliable.

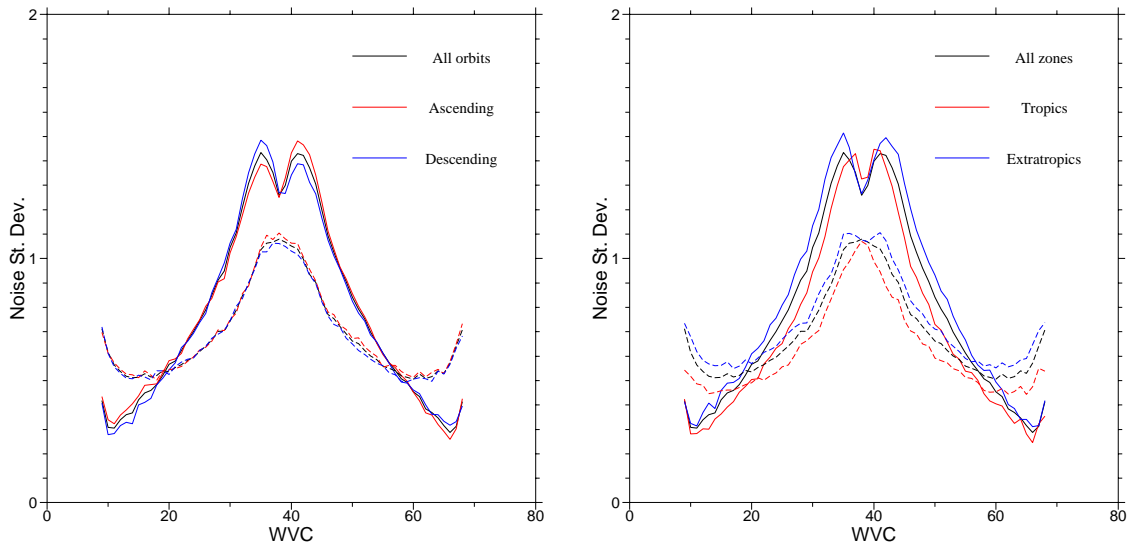


**Figure 4.5** Standard deviation of the noise level in the SDP wind speed components  $u$  (solid curves) and  $v$  (dashed curves) for various orbit selections (left) and geographical zones (right).

#### 4.4 Minimization routine

Figure 4.6 shows the standard deviation of the noise level in the SDP retrieved wind speed components  $u$  and  $v$  for two choices of the minimization routine in the 2DVAR ambiguity removal scheme. Originally, SDP used routine N1QN3, but this routine was replaced by the freeware routine LBFGS of J. Nocedal [Liu and Nocedal, 1989]. Routine LBFGS finds lower minima in the 2DVAR cost function than N1QN3 [Scat group, 2006b]. This means that the wind vector solution obtained with LBFGS lies closer to the observations and deviates more from the initial model wind field than that obtained with N1QN3. One therefore expects more noise in the LBFGS solutions. Figure 4.6 shows, however, little difference between the two minimization routines.

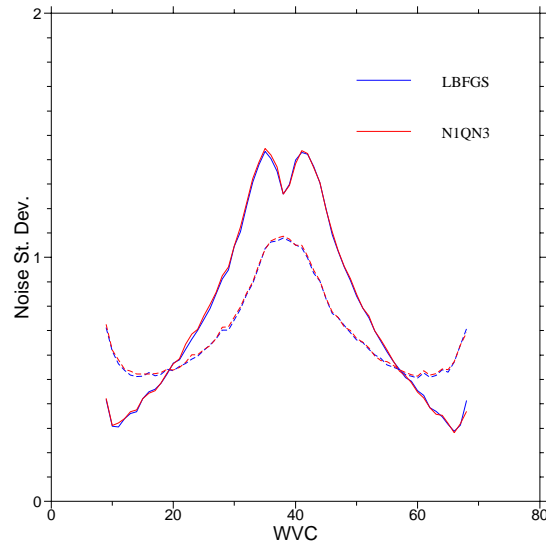


**Figure 4.6** Standard deviation of the noise level in the wind speed components  $u$  (solid curves) and  $v$  (dashed curves) for minimization routine LBFGS (blue curves) and N1QN3 (red curves).

#### 4.5 MSS

SDP can apply the Multiple Solution Scheme (MSS). Rather than selecting only (local) minima of the inversion cost function, the MSS retains all likely wind vector solutions (currently up to 144), each of which has assigned a probability depending on its value of the inversion cost function. The MSS may select solutions that do not coincide with a local maximum in the local inversion probability, that but still have a relatively high probability of being the correct solution.

<b>NWP SAF</b>	<b>On the quality of high resolution wind fields</b>	Doc ID : NWPSAF-KN-TR-002 Version : 1.2 Date : 31-08-2006
----------------	--	---

Application of the MSS in combination with 2DVAR should result in a smoother solution, because 2DVAR acts as a meteorologically balanced spatial filter.

Figure 4.7 shows that this is indeed the case. The left panel shows the standard deviation, the right panel the variance of the noise contribution. The red curves were obtained using quadratic extrapolation for estimating the noise peak height. For the MSS, this yields small, negative values and the corresponding standard deviations are set to zero (red curves in figure 4.7). Application of a Gaussian fit, which tends to overestimate the noise level, yields small positive values for the noise level (blue curves).

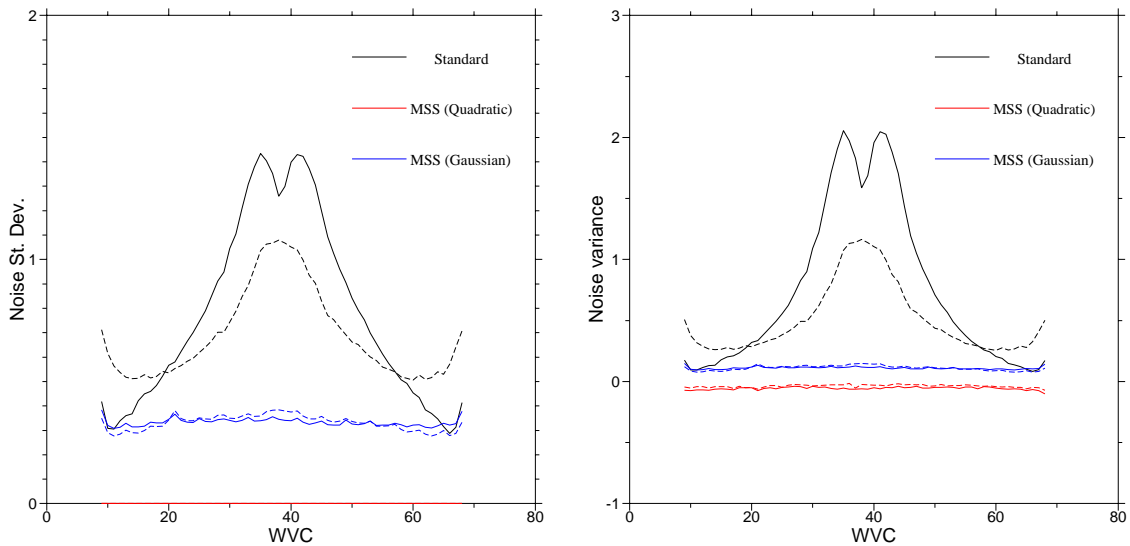


**Figure 4.7** Standard deviation (left) and variance (right) of the noise level in the SDP wind speed components  $u$  (solid curves) and  $v$  (dashed curves) for the standard four-solution scheme (black curves) and the MSS (blue and red curves). The red curves were obtained using quadratic extrapolation to assess the noise peak height; the blue curves using a Gaussian fit.

As stated earlier, the noise level contains two errors: a stochastic error with a variance of about  $0.03 \text{ m}^2/\text{s}^2$  for quadratic extrapolation (see section 4.1), and a systematic error due to the extrapolation method used. The variances obtained with the MSS (blue and red curves in the right hand panel of figure 4.7) show both errors: the wiggle in the curves is due to the stochastic error which has the expected order of magnitude, while the gap between the blue and red curves is due to a systematic error induced by the extrapolation method. The gap has a width of about  $0.2 \text{ m}^2/\text{s}^2$ ,

<b>NWP SAF</b>	<b>On the quality of high resolution wind fields</b>	Doc ID : NWPSAF-KN-TR-002 Version : 1.2 Date : 31-08-2006
----------------	--	---

and noise variance levels of this order or smaller can be regarded upon as not significant. It can thus be concluded that the MSS is very effective in reducing the noise in the wind field.

## 4.6 Resolution

SDP has the possibility to produce wind fields at a resolution of 25 km, 50 km, and 100 km [*Scat group*, 2006a]. The accuracy of the 100 km resolution product has been checked by comparing with ECMWF First Guess at Appropriate Time (FGAT) wind fields. For wind fields with higher resolution such a comparison is not possible, because the difference in resolution becomes too large.

One may, however, expect that the noise level decreases with increasing wind vector cell size, because of the spatial integration of the basic backscatter measurements. As such, a wind vector cell in the 50 km product is the average of  $2 \times 2$  wind vector cells at 25 km size. Similarly, a wind vector cell in the 100 km product is the average of  $4 \times 4$  cells at 25 km resolution.

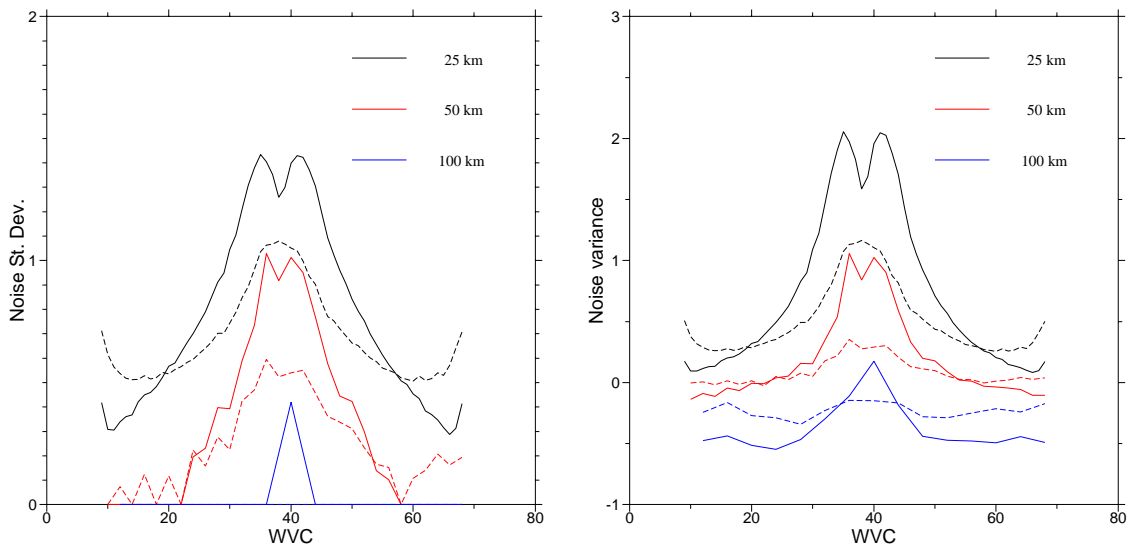


**Figure 4.8** Standard deviation (left) and variance (right) of the noise level in the SDP wind speed components  $u$  (solid curves) and  $v$  (dashed curves) at various resolutions.

Figure 4.8 shows the standard deviation (left) and the variance (right) of the noise level in the scatterometer wind speed components  $u$  and  $v$  as a function of WVC number for various

<b>NWP SAF</b>	<b>On the quality of high resolution wind fields</b>	Doc ID : NWPSAF-KN-TR-002 Version : 1.2 Date : 31-08-2006
----------------	--	---

resolutions. Because the swath width remains the same, the number of WVC's depends on the resolution cell size according to table 4.1.

<b>Resolution cell size (km)</b>	<b>Number of resolution cells</b>
25	76
50	38
100	19

**Table 4.1** Resolution cell size and number of resolution cells for SDP output.

At 25 km resolution cell size (black curves) the WVC number on the x-axis corresponds to the actual WVC number. For resolution cell sizes of 50 km (red curves) and 100 km (blue curves) the WVC number has been multiplied by 2 and 4, respectively, in order to arrive at the same range of WVC number for each resolution.

Figure 4.8 shows that the noise level roughly decreases with a factor of two when the resolution cell doubles in size. It should be noted here that the systematic error may vary with resolution, because the separation between the support points for extrapolation increases with resolution. At 100 km resolution little noise is detected: estimation of the noise peak height with quadratic extrapolation yields a negative value in most cases. This indicates that the noise level at 100 km resolution is hardly statistically significant, except for extreme nadir viewing.

NWP SAF	<b>On the quality of high resolution wind fields</b>	Doc ID : NWPSAF-KN-TR-002 Version : 1.2 Date : 31-08-2006
---------	--	---

# 5 Results for the spectrum

## 5.1 Comparison of methods

Figure 5.1 shows the spectra for the scatterometer and model wind speed components  $u$  and  $v$ , obtained with the following methods:

- FFT of the raw autocorrelation including the noise peak at zero distance (blue);
- FFT of the autocorrelation without noise peak (removed using quadratic extrapolation) smoothed using the smoothing spline routine GCVSPL [Woltring, 1986] (red).
- FFT of the spline smoothed autocorrelation without noise peak applying a Hanning window (green).

The spectra of the scatterometer wind components obtained from Fourier transforming the raw autocorrelations (blue curves in figure 5.1) tend to move more horizontal at high spatial frequencies. This is due to the noise peak in the autocorrelation which transforms to a constant contribution in the spectrum. It is absent for the model winds. Note that the spectra become noisier at low levels, in particular for the spectrum of the model wind speed at spectral densities below  $10^{-8}$ .

When the noise peak is removed and the autocorrelation is smoothed with a spline fit (red curves), the spectra of the scatterometer winds become steeper, though there is still some horizontal flattening at high spatial frequencies. This resembles the behavior in figure 2.4, and is most probably due to aliasing. The model wind speed spectra are relatively unaffected by smoothing, but remain very noisy at low levels

Applying a Hanning filter after noise peak removal and spline smoothing (green curves) results in relatively smooth spectra. The spectral level is slightly increased because of normalization differences. When applying the Hanning window, the model wind speed spectra show a dip at spatial frequencies around  $k_{25} \approx 0.4 \cdot 10^{-5}$ , corresponding to a distance of 250 km, the known spectral cut-off of NWP models. This will be discussed further in the next section.

At  $k \approx 10^{-5}$  (distance of the order of 100 km), the scatterometer wind fields generally contain an order of magnitude more spectral density than the model fields. This is consistent with the more rapid decrease near the origin of the autocorrelation function of scatterometer winds.

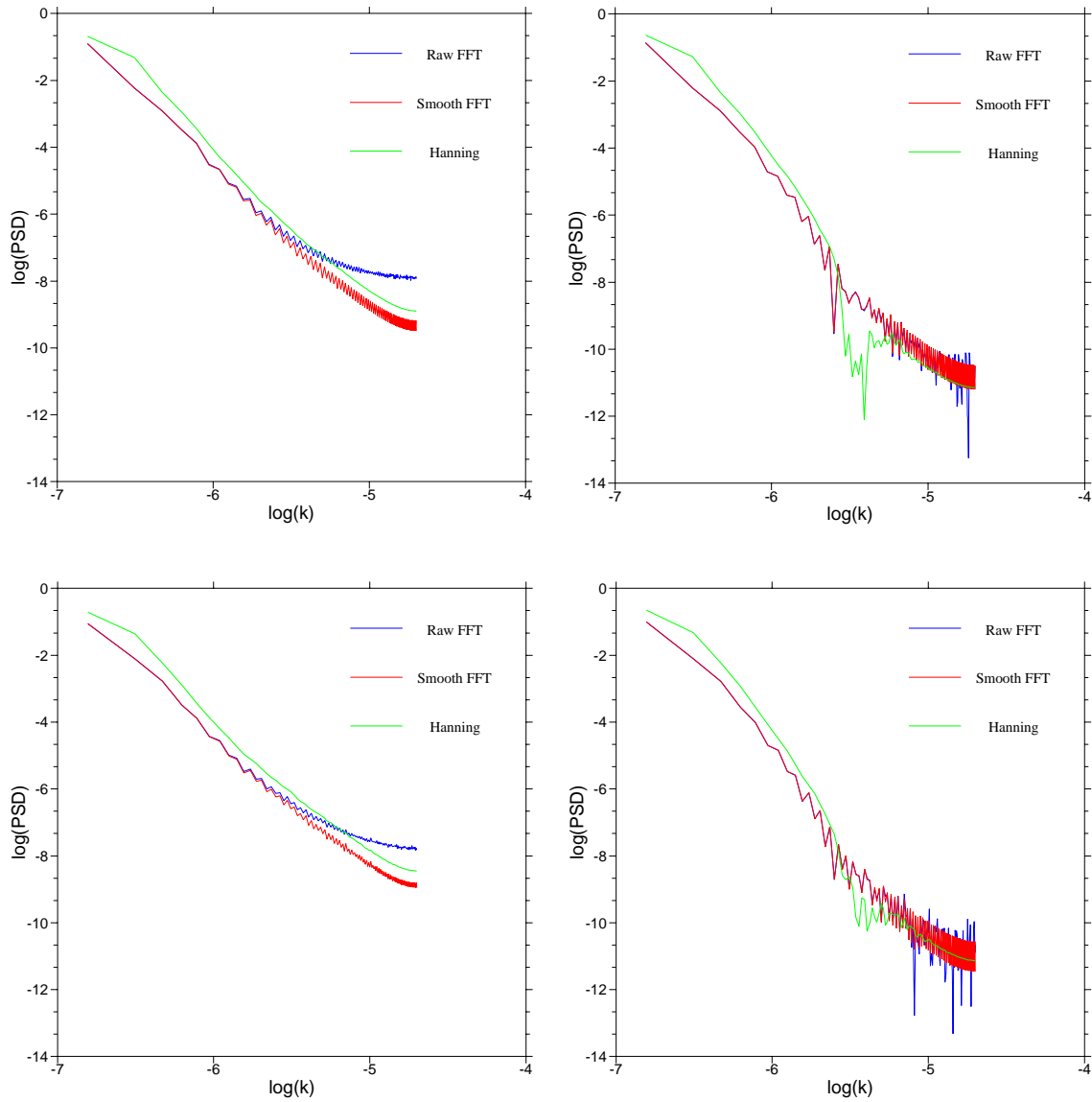


**Figure 5.1** Spectra of the scatterometer (left) and model (right) wind speed components  $u$  (upper) and  $v$  (lower), obtained with various methods indicated in the text.

## 5.2 Window functions

In the previous section it was shown that application of a Hanning window resulted in much smoother spectra obtained with FFT methods. Figure 5.2 shows the results obtained with other popular window functions, Welch and Parzen, and the so-called zero window which is obtained by setting all autocorrelations to zero after the first zero of the autocorrelation.

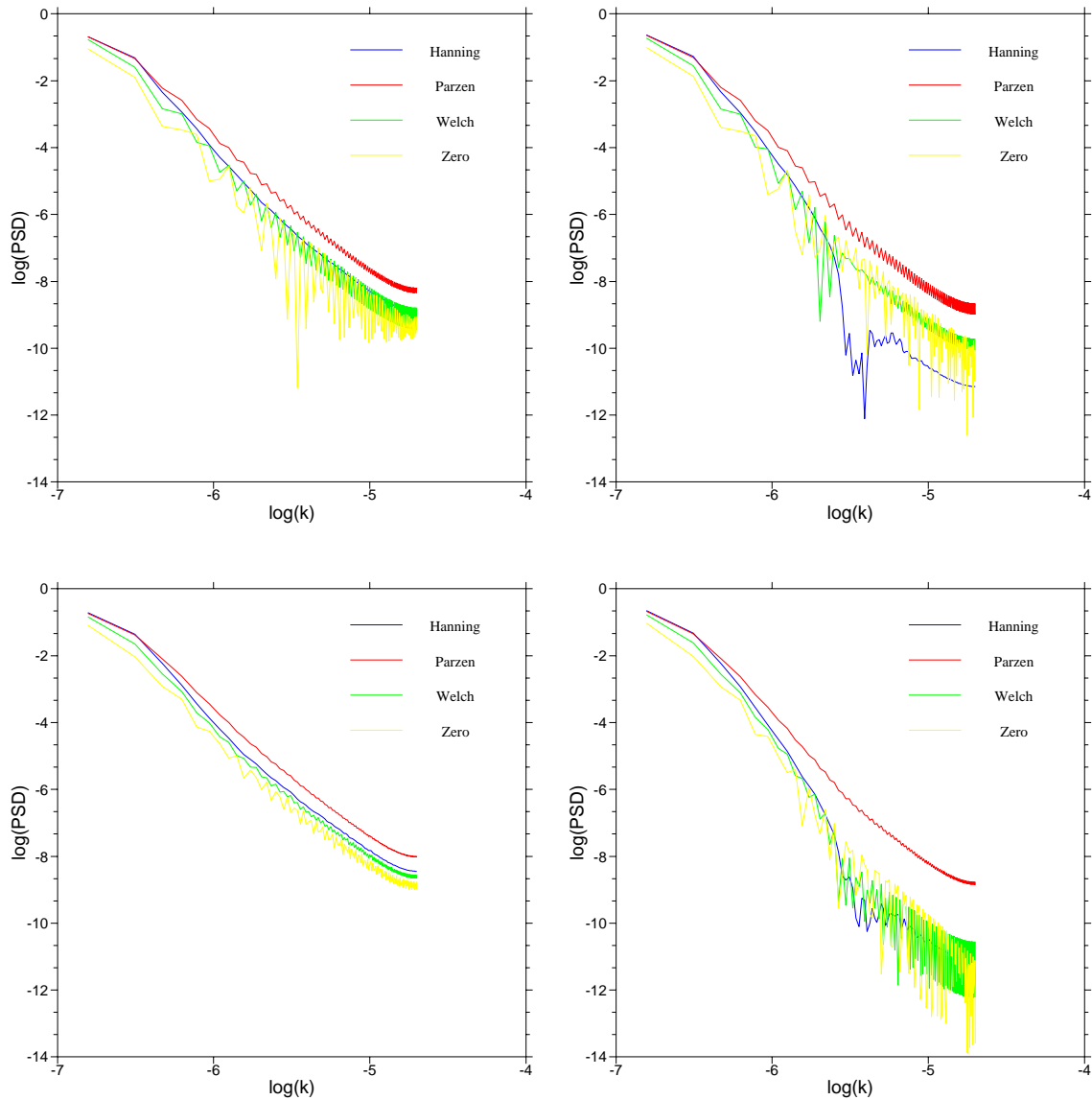


**Figure 5.2** Spectra of the scatterometer (left) and model (right) wind components  $u$  (upper) and  $v$  (lower) for various windowing functions. See the text for details.

Figure 5.2 shows that the Hanning filter has the best smoothing properties. The Parzen and Welch window functions give some smoothing, but the spectra at high spatial frequencies contains an oscillation. The zero window gives no improvement.

Note that only the Hanning window shows the dip in spectral densities at  $k \approx 0.4 \cdot 10^{-5}$ , corresponding to a distance of 250 km, the known cutoff length of NWP models. Since the other window functions do not show this dip, it is probably a numerical artifact caused by interference

<b>NWP SAF</b>	<b>On the quality of high resolution wind fields</b>	Doc ID : NWPSAF-KN-TR-002 Version : 1.2 Date : 31-08-2006
----------------	--	---

between the harmonic induced by the Hanning filter and those caused by the finite integration interval (see section 2.4). However, all curves in the right hand panel of figure 5.2 exhibit a change in slope for  $k \approx 0.4 \cdot 10^{-5}$ , which may be attributed to the cutoff of the NCEP model.

## 6 Comparison with DIRTH

The standard level 2 SeaWinds wind fields as delivered by NOAA are at a grid size of 25 km and have their ambiguity removed with the “Directional Interval Retrieval with Thresholded Nudging” (DIRTH) method [Stiles *et al.*, 2002]. This method is based on the median filter and uses the NCEP model wind predictions for initialization, just like 2DVAR.

The noise level in the standard Seawinds data product has been calculated using the methods developed in the previous chapters. The results for the noise standard deviation and variance in the wind components  $u$  and  $v$  at 25 km resolution are shown in figure 6.1. The noise peak height was estimated using quadratic extrapolation.

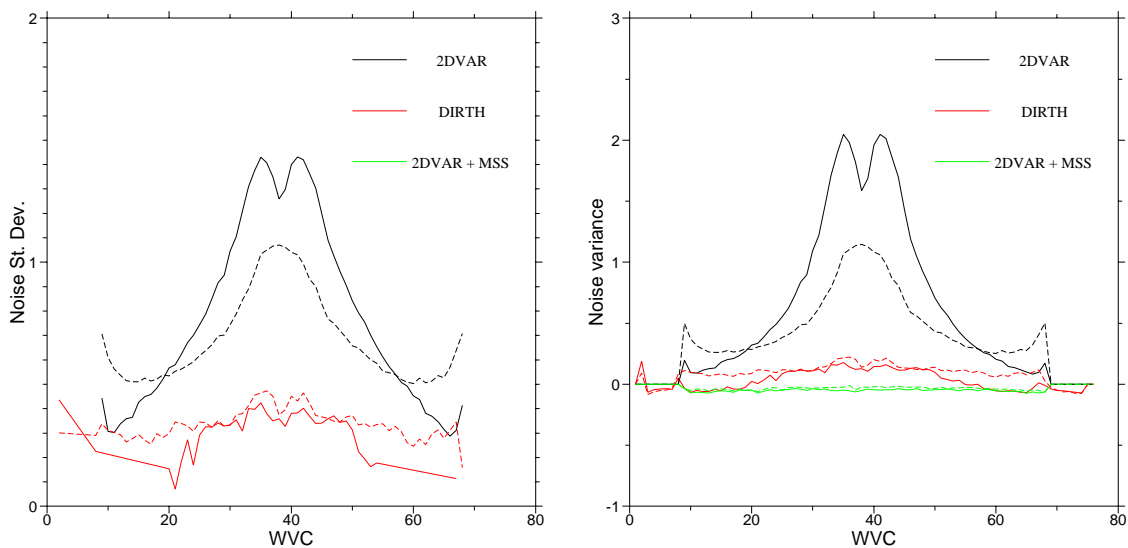


Figure 6.1 Standard deviation (left panel) and variance (right panel) of the noise level against WVC number. Solid curves: zonal wind component  $u$ ; dashed curves: meridional wind component  $v$ . Black curves: 2DVAR without MSS; red curves: DIRTH; green curves: 2DVAR with MSS.

Without MSS, the 2DVAR scheme generates high noise levels as shown by the black curves in figure 6.1. These curves are the same as already shown in chapter 4.

The DIRTH scheme (red curves) performs quite well: it causes a small white noise component with a standard deviation of 0.47 m/s at most. The noise level is highest in the nadir part of the swath, though less pronounced as for the 2DVAR results without MSS. Note that the standard

<b>NWP SAF</b>	<b>On the quality of high resolution wind fields</b>	Doc ID : NWPSAF-KN-TR-002 Version : 1.2 Date : 31-08-2006
----------------	--	---

level 2 SeaWinds product also gives some results for the outer swaths (WVC 1-8 and 69-76). These WVC's are rejected by SDP.

Though DIRTH performs quite well, it still contains some noise. Only application of the 2DVAR ambiguity removal with MSS (green curves) removes the noise below its detection level. Since quadratic extrapolation overshoots the autocorrelation slightly at zero distance, only small negative values of the variance are found and, hence, no values for the standard deviation.

NWP SAF	<b>On the quality of high resolution wind fields</b>	Doc ID : NWPSAF-KN-TR-002 Version : 1.2 Date : 31-08-2006
---------	--	---

## 7 Outlook to the Future

The two-dimensional variational ambiguity removal (2DVAR) method selects the wind solution that fits best with a model wind field under the additional constraint that it should obey the meteorological balance [Stoffelen *et al.*, 2000]. The present implementation of the 2DVAR method within genscat employs minimization of a cost function in the spatial frequency domain (rather than the spatial domeain). The advantage of this approach is that convolutions in the spatial domain transform to multiplications in the frequency domain.

The spatial structure of the wind field is in 2DVAR constrained by physical laws. This is incorporated in structure functions (also called covariance functions) that are defined in the frequency domain. At the moment , 2DVAR contains quasi geostrophic structure functions that are derived from the basic equations of motion. When expressed in terms of longitudinal and transversal components, the quasi-geostrophic structure functions contain two adjustable parameters: one describing the size of the structures and one controlling the amount of geostrophic adherence.

In principle, the structure functions could also be obtained from the analysis field (the wind field that 2DVAR calculates from the observations as a correction to the model wind field). This is called the observational method [Stoffelen *et al.* 2000]. This method also requires that the structure functions are described in terms of longitudinal and transverse components.

Considering the observation geometry of SeaWinds (or any other scatterometer), the longitudinal component is directed parallel to the satellite motion and is equivalent to the wind speed component  $T$  defined in (3.1). Similarly, the transverse component is directed perpendicular to the satellite motion and is equivalent to the wind speed component  $P$ . Therefore further analysis on the autocorrelation of  $P$  and  $T$  may yield information on the nature of the structure functions. This is one of the remaining tasks within the NWP SAF project.

Note that  $T$  is not the transverse component, but the longitudinal or parallel one, the component tangential to the curved satellite orbit. Note also that  $P$  is the wind component perpendicular to the satellite motion, not parallel.

<b>NWP SAF</b>	<b>On the quality of high resolution wind fields</b>	Doc ID : NWPSAF-KN-TR-002 Version : 1.2 Date : 31-08-2006
----------------	--	---

NWP SAF	<b>On the quality of high resolution wind fields</b>	Doc ID : NWPSAF-KN-TR-002 Version : 1.2 Date : 31-08-2006
---------	--	---

## 8 Conclusions

The quality of high resolution scatterometer wind fields as retrieved with the SeaWinds Data Processor (SDP) has been studied in the framework of the NWP SAF project funded by EUMETSAT. The study focused on the statistical properties of the retrieved wind fields, notably the autocorrelation function and the spectrum.

The following conclusions may be drawn from this study:

1. A white noise contribution in the wind field causes a discontinuity in the autocorrelation at zero distance, the so-called noise peak. The variance of the noise level equals the height of the noise peak times the total variance of the wind field.
2. A simple quadratic extrapolation is generally sufficient to estimate the height of the noise peak. If the noise level is very small or zero, quadratic extrapolation may overshoot the extrapolated autocorrelation at zero distance, leading to small negative values for the noise peak height.
3. A white noise contribution causes the wind spectrum to flatten at large spatial frequencies. However, aliasing causes the same behaviour. Aliasing can only be removed by carefully considering the autocorrelations up to such distances that it approaches zero. However, this is infeasible in practice, because the autocorrelation approaches zero only very slowly due to the large world-wide flow regimes. Therefore, the wind spectrum has little added value in studying wind products as compared to a basic autocorrelation analysis.
4. The noise level is highest in the nadir part of the swath. Its standard deviation may be up to 1.4 m/s in the zonal component  $u$  and 1.1 m/s in the meridional component  $v$ , at 25 km resolution.
5. The noise level decreases with increasing wind vector cell size, and becomes negligible at 100 km cell size. On the other hand, one may expect a further increase in the noise level for wind vector cells smaller than 25 km.
6. The noise can be reduced when using the DIRTH scheme for ambiguity removal, or completely removed when using KNMI's 2DVAR scheme in combination with MSS.
7. The statistical methods developed in this study may be used to improve the implementation of the structure functions in the 2DVAR method.

<b>NWP SAF</b>	<b>On the quality of high resolution wind fields</b>	Doc ID : NWPSAF-KN-TR-002 Version : 1.2 Date : 31-08-2006
----------------	--	---

<b>NWP SAF</b>	<b>On the quality of high resolution wind fields</b>	Doc ID : NWPSAF-KN-TR-002 Version : 1.2 Date : 31-08-2006
----------------	--	---

# References

- Chelton, D.B., Freilich, M.H., Sienkiewicz, J.M., and Von Ahn, J.N., 2006  
On the use of QuikSCAT scatterometer measurements of surface winds for marine weather prediction.  
*Monthly Weather Review*, 134, pp. 2055-2071.
- Isaaks, E.H., and Mohan Srivastava, R., 1989  
*Applied Geostatistics*.  
Oxford University Press, New York, USA.
- Liu, D.C., and Nocedal, J., 1989  
On the limited memory BFGS method for large scale optimization methods.  
*Mathematical Programming*, 45, pp 503-528.
- Milliff, R.F., 2004,  
*Comparing the kinetic energy vs. wavenumber in surface wind fields from ECMWF analyses and the NASA QuikSCAT scatterometer*. Report to Instituto Nazionale di Geofisica e Vulcanologia.
- Press, W.H., Flannery, B.P., Teukolsky, S.A., and Vetterling, W.T., 1988,  
*Numerical Recipes*. Cambridge University Press, Cambridge, USA.
- SCAT group (De Kloe, J., Stoffelen, A, Portabella, M, Verhoef, A., Verspeek, J., and Vogelzang, J., 2006a,  
*SDP User Manual and Reference Guide*. Report NWPSAF-KN-UD-002, KNMI, Netherlands.
- SCAT group (De Kloe, J., Stoffelen, A, Portabella, M, Verhoef, A., Verspeek, J., and Vogelzang, J., 2006b,  
*SDP Test Report*. Report NWPSAF-KN-TV-002, KNMI, Netherlands.
- Stiles, B.W., Pollard, B.D., and Dunbar, R.S., 2002,  
Directional interval retrieval with thresholded nudging. *IEEE Transactions on Geoscience and Remote Sensing*, 40, pp 79-89.
- Stoffelen, A., de Vries, J., and Voorrips, A., 2000,  
*Towards the real-time use of QuikSCAT winds*.  
Report USP-2/00-26, Netherlands Remote Sensing Board, Delft, The Netherlands.
- Woltring, H.J., 1986,  
A FORTRAN package for generalized, cross-validatorspline smoothing and differentiation.  
*Advances in Engineering Software*, 8 (2) 104-113.